**Astronomy**
**&**
**Astrophysics**

# The remarkable solar twin HIP 56948: a prime target in the quest for other Earths[*],[**]

J. Meléndez[1], M. Bergemann[2], J. G. Cohen[3], M. Endl[4], A. I. Karakas[5], I. Ramírez[4,6], W. D. Cochran[4], D. Yong[5], P. J. MacQueen[4], C. Kobayashi[5,***], and M. Asplund[5]

[1] Departamento de Astronomia do IAG/USP, Universidade de São Paulo, Rua do Matão 1226, Cidade Universitária, 05508-900 São Paulo, SP, Brazil
e-mail: jorge@astro.iag.usp.br
[2] Max Planck Institute for Astrophysics, Postfach 1317, 85741 Garching, Germany
[3] Palomar Observatory, Mail Stop 105-24, California Institute of Technology, Pasadena, California 91125, USA
[4] McDonald Observatory, The University of Texas at Austin, Austin, TX 78712, USA
[5] Research School of Astronomy and Astrophysics, The Australian National University, Cotter Road, Weston, ACT 2611, Australia
[6] The Observatories of the Carnegie Institution for Science, 813 Santa Barbara Street, Pasadena, CA 91101, USA

## ABSTRACT

*Context.* The Sun shows abundance anomalies relative to most solar twins. If the abundance peculiarities are due to the formation of inner rocky planets, that would mean that only a small fraction of solar type stars may host terrestrial planets.
*Aims.* In this work we study HIP 56948, the best solar twin known to date, to determine with an unparalleled precision how similar it is to the Sun in its physical properties, chemical composition and planet architecture. We explore whether the abundances anomalies may be due to pollution from stellar ejecta or to terrestrial planet formation.
*Methods.* We perform a differential abundance analysis (both in LTE and NLTE) using high resolution ($R \sim 100\,000$) high S/N (600–650) Keck HIRES spectra of the Sun (as reflected from the asteroid Ceres) and HIP 56948. We use precise radial velocity data from the McDonald and Keck observatories to search for planets around this star.
*Results.* We achieve a precision of $\sigma \lesssim 0.003$ dex for several elements. Including errors in stellar parameters the total uncertainty is as low as $\sigma \simeq 0.005$ dex (1%), which is unprecedented in elemental abundance studies. The similarities between HIP 56948 and the Sun are astonishing. HIP 56948 is only $17 \pm 7$ K hotter than the Sun, and $\log g$, [Fe/H] and microturbulence velocity are only $+0.02 \pm 0.02$ dex, $+0.02 \pm 0.01$ dex and $+0.01 \pm 0.01$ km s$^{-1}$ higher than solar, respectively. Our precise stellar parameters and a differential isochrone analysis shows that HIP 56948 has a mass of $1.02 \pm 0.02\ M_\odot$ and that it is ~1 Gyr younger than the Sun, as constrained by isochrones, chromospheric activity, Li and rotation. Both stars show a chemical abundance pattern that differs from most solar twins, but the refractory elements (those with condensation temperature $T_{\rm cond} \gtrsim 1000$ K) are slightly (~0.01 dex) more depleted in the Sun than in HIP 56948. The trend with $T_{\rm cond}$ in differential abundances (twins − HIP 56948) can be reproduced very well by adding ~3 $M_\oplus$ of a mix of Earth and meteoritic material, to the convection zone of HIP 56948. The element-to-element scatter of the Earth/meteoritic mix for the case of hypothetical rocky planets around HIP 56948 is only 0.0047 dex. From our radial velocity monitoring we find no indications of giant planets interior to or within the habitable zone of HIP 56948.
*Conclusions.* We conclude that HIP 56948 is an excellent candidate to host a planetary system like our own, including the possible presence of inner terrestrial planets. Its striking similarity to the Sun and its mature age makes HIP 56948 a prime target in the quest for other Earths and SETI endeavors.

**Key words.** Sun: abundances – stars: abundances – stars: fundamental parameters – Earth – meteorites, meteors, meteoroids – planet-star interactions

## 1. Introduction

In recent years there has been an important number of studies related to solar twins, stars which are spectroscopically almost identical to the Sun. The reader is referred to Cayrel de Strobel (1996) for a review of the early history regarding the search for solar twins, that culminated with the identification of 18 Sco as the closest ever solar twin (Porto de Mello & da Silva 1997; Soubiran & Triaud 2004). More recently, new solar twins have been identified (Meléndez et al. 2006; Meléndez & Ramírez 2007; Takeda et al. 2007; Pasquini et al. 2008; Takeda & Tajitsu 2009; Meléndez et al. 2009; Ramírez et al. 2009) and HIP 56948 has demoted 18 Sco as the star that most closely resembles the Sun (Meléndez & Ramírez 2007; Takeda & Tajitsu 2009).

Solar twins are useful to calibrate the zero-points of the temperature (Casagrande et al. 2010; Meléndez et al. 2010b; Ramirez et al. 2012) and metallicity (Meléndez et al. 2010b; Casagrande et al. 2011) scales, to better characterize the interiors of stars like the Sun (Bazot et al. 2011), and to identify

---

the transport mechanisms that cause Li depletion in the Sun (do Nascimento et al. 2009; Meléndez et al. 2010a; Baumann et al. 2010; Denissenkov 2010; Castro et al. 2011; Li et al. 2012). But most importantly, solar twins are the perfect targets to look for small chemical abundance anomalies that may have been unnoticed in previous works (Gustafsson 2008; Gustafsson et al. 2010).

The first spectroscopic study designed to exploit the advantages of a differential abundance analysis between solar twins and the Sun, showed that our Sun has a peculiar chemical abundance pattern, suggested to arise from accretion of material depleted in refractory elements due to the formation of terrestrial planets (Meléndez et al. 2009). Further studies have confirmed, with different degrees of accuracy, that the Sun indeed has an anomalous surface composition (Ramírez et al. 2009, 2010; Gonzalez et al. 2010; González Hernández et al. 2010)[1]. We show in Appendix A, that the reality of these abundance anomalies is well established. Besides the important implications for planet formation (Chambers 2010) and to explain abundance anomalies in Jupiter (Nordlund 2009), the solar abundance peculiarities may be relevant for modeling early stellar evolution (Baraffe & Chabrier 2010) and for solving the solar modelling crisis when using low solar abundances (Nordlund 2009; Guzik & Mussack 2010).

Even before the deficiency of refractory elements in the solar convection zone was discovered, Castro et al. (2007) investigated the effect of accretion of metal-poor material onto the Sun as a way to help solve the solar modelling problem when a low oxygen abundance (Allende Prieto et al. 2001; Asplund et al. 2004; Meléndez & Asplund 2008) is adopted, and they found that indeed accretion provides some improvement, but the problem is not fully solved. Guzik & Mussack (2010) demonstrated an improvement in the comparison between stellar models and helioseismic data when accretion of low-Z material is taken into account (their Fig. 9), albeit a full resolution of the discrepancy is not found. More detailed modelling has been recently presented by Serenelli et al. (2011), who use up-to-date nuclear cross-sections and include accretion of metal-poor and metal-rich material, considering a range of accreted mass and different timings for accretion. They conclude that there is somewhat better agreement with helioseismology for differentiated accretion, but not complete agreement. Overall, models with metal-poor accretion improve the agreement with the helium abundance inferred from helioseismology, while metal-rich accretion improves both the depth of the convection zone and the sound speed profile, with exception of a model with late accretion of 0.015 $M_\odot$ of metal-poor material, which improves the agreement with the sound speed profile.

A detailed test of the terrestrial planet formation hypothesis was performed by Chambers (2010), who used the composition of about two dozen chemical elements in the Earth and CM chondrites (representative of the asteroid belt). Interestingly, Chambers (2010) showed that Earth material alone can not fully explain the peculiar solar pattern, but that a mix of Earth and meteoritic material gives an excellent fit for more than 20 chemical elements. Thus, the peculiarities in the Sun could be a signature of both the formation of terrestrial planets and of the asteroid belt.

An interesting alternative interpretation of the solar abundance anomalies, from an analysis of the solar twin M 67-1164 (Önehag et al. 2011), is that the chemical peculiarities may reflect that the Sun was born in a massive open cluster like M 67. Using various arguments, Adams (2010) concludes that the birth environment of the solar system might be a moderately large cluster with $10^3$–$10^4$ members. Nevertheless, only one solar twin in M 67 has been analyzed to date for high precision chemical abundances (Önehag et al. 2011), so, more observations are urgently needed to verify if indeed all solar twins in M 67 have the same solar abundance pattern. Also, notice that based on a dynamical study, Pichardo et al. (2012) have shown that the Sun could not have been born in M 67.

Gustafsson et al. (2010) warned about potential systematic effects in chemical abundances due to different lines of sights when the Sun is compared to the solar twins. Kiselman et al. (2011) have recently studied the line-of-sight effect using high resolution observations at the solar equator and at latitude 45°. Seven key chemical elements in a broad range of condensation temperature were analyzed by Kiselman et al. (2011), who show that there is no difference in the abundances obtained at different latitudes for both volatile (to within 0.005 dex) and refractory (to within 0.002 dex) elements. Thus, it is very unlikely that the abundance anomalies seen in the Sun (Meléndez et al. 2009; Ramírez et al. 2009) can be attributed to line-of-sight inclination effects.

In Appendix B, we show that the Sun's chemical peculiarities also do not arise due to the particular reflection properties of the asteroids employed in the analyses, as expected given that the relative reflectance of asteroids show mostly smooth changes over hundreds of Å (e.g. Xu et al. 1995; Binzel et al. 1996; Bus & Binzel 2002; Lazzaro et al. 2004; DeMeo et al. 2009), about 3 orders of magnitude wider than the narrow stellar lines used in abundance analyses.

Only some 15% of solar type stars appear chemically similar to the Sun (Meléndez et al. 2009; Ramírez et al. 2009) and therefore we regard the Sun to have an anomalous chemical abundance when compared to other solar twins. Assuming that the solar abundance anomalies are due to terrestrial planet formation, then perhaps only these 15% of solar type stars that are chemically similar to the Sun may host rocky planets. This is a lower limit to the amount of rocky planets formed around other Suns, as part of those planets may fall into their host stars, thus altering the original abundance signature. The Kepler mission (e.g. Borucki et al. 2010) will give us the first estimate of the frequency of Earth-sized planets in the habitable zones of solar type dwarfs.

It is important now to find, through a detailed chemical abundance analysis, stars which are chemically identical to the Sun and which may therefore potentially host other Earths. HIP 56948[2] is the perfect candidate for identifying subtle chemical anomalies, as this star has been found to be the most similar to the Sun in stellar parameters (Meléndez & Ramírez 2007; Takeda & Tajitsu 2009). The first high precision ($\sigma \sim 0.03$ dex) detailed abundance analysis of this star showed that HIP 56948 may be one of the rare stars with a solar abundance pattern (Ramírez et al. 2009). In the present work, we perform a much more refined study ($\sigma \sim 0.005$ dex) of HIP 56948, to assess its similarity to the Sun and to which extent it may host a planetary system like ours.

---

[1] González Hernández et al. (2010) have contested the planet signature scenario, but further scrutiny of their work by Ramírez et al. (2010) demonstrated that in fact the results of González Hernández et al. are fully consistent with the works of Meléndez et al. (2009) and Ramírez et al. (2009).

[2] a.k.a. *Intipa Awachan*,
http://tierneylab.blogs.nytimes.com/?s=intipa

**Fig. 1.** Comparison of HIP 56948 (red circles) and the Sun (solid line) in different spectral regions. The quality of the Keck/HIRES spectra is very high for both HIP 56948 ($S/N \sim 600$) and the Sun ($S/N \sim 650$). It is hard to distinguish any difference between the stars.

## 2. Observations

### 2.1. Keck HIRES spectra for high precision abundance analysis

HIP 56948 and the Sun (reflected light from the Ceres asteroid) were observed with HIRES (Vogt et al. 1994) at the Keck I telescope on May 19, 2009. Exactly the same setup was used for both HIP 56948 and Ceres, and the asteroid was observed immediately after HIP 56948. A total exposure time of 800 s was used for both HIP 56948 and the Sun, consisting of multiple observations co-added, in order to avoid non-linearity. We stress here that for highly accurate work an asteroid should be used instead of the daytime skylight, as there are important variations in the skylight spectrum with respect to the solar spectrum (Gray et al. 2000). Furthermore, asteroids are essentially point sources for typical observing conditions (seeing >0.5 arcsec), thus the observation and data reduction for both stars and the asteroid are performed in the same way.

A resolving power of $R \approx 10^5$ was achieved using the E4 0.4″-wide slit, accepting some light loss (seeing was ~0.7 arcsec) in order to achieve the necessary spectral resolution. For HIP 56948 the signal-to-noise level measured in continuum regions is about 600 per pixel at 6000 Å, while it is somewhat better ($S/N = 650$) for Ceres, for which the predicted magnitude at the time of the observation was $V = 8.30$[3], i.e., somewhat brighter than HIP 56948 ($V = 8.671 \pm 0.004$, Olsen 1993; Ramírez et al. 2012).

The spectral orders were extracted using MAKEE[4]. Further data reductions (Doppler correction, continuum normalization, and combining spectra) were performed with IRAF. A comparison of the reduced spectra of HIP 56948 and the Sun is shown in Fig. 1. As can be seen, the spectra are nearly indistinguishable.
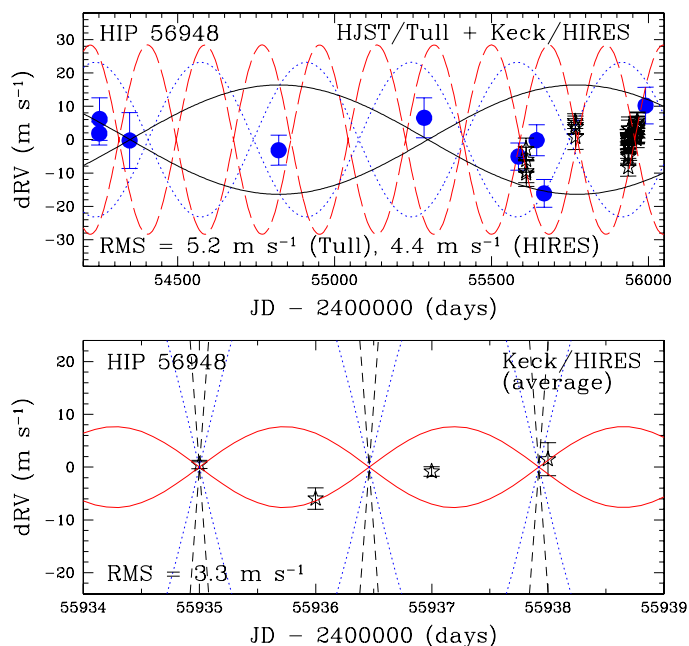
---

[3] http://ssd.jpl.nasa.gov/horizons.cgi
[4] MAKEE was developed by T. A. Barlow specifically for reduction of Keck HIRES data. It is freely available at http://www2.keck.hawaii.edu/realpublic/inst/hires/data_reduction.html



**Fig. 2.** *Upper panel:* precise radial velocities obtained with the Tull Coude Spectrograph at the 2.7 m Harlan J. Smith Telescope (HJST) of the McDonald Observatory (filled circles) and with the HIRES spectrograph at the 10 m Keck telescope (stars). We show some circular orbits for a Jupiter-mass planet at 1 AU (long dashed line), 1.5 AU (dotted line) and 3 AU (solid line). *Lower panel:* average of three short (3-min) consecutive observations taken with HIRES/Keck during four nights in January 2012. Some circular orbits due to hypothetical Neptune-mass (solid line), Saturn-mass (dotted line) and Jupiter-mass (dashed line) planets at 0.04 AU, are shown for comparison. No giant planets have been detected so far in the inner regions (<3 AU) around HIP 56948.

### 2.2. McDonald and Keck radial velocities for planet search

Soon after HIP 56948 was identified as the best solar twin (Meléndez & Ramírez 2007), the McDonald Observatory planet search program (e.g., Endl et al. 2006; Robertson et al. 2012) began to monitor this star. The observations have been carried out with the Tull Coude Spectrograph (Tull et al. 1995) at the 2.7m Harlan J. Smith Telescope. HIP 56948 has so far been observed nine times (from May 2007 to March 2012) and the scatter of the observations is 5.2 m s$^{-1}$ (discarding one outlier), which is consistent with the 5.1 m s$^{-1}$ median error bar. The radial velocity data are presented in Table 1 and Fig. 2.

In February 2011 we started observing HIP 56948 for planets using HIRES at Keck during time allocated to a NASA key science program to support the CoRoT mission[5]. We have acquired 30 datapoints with HIRES up to February 2012. The radial velocity data are presented in Table 2 and Fig. 2.

For both instruments we use a temperature-controlled iodine cell for wavelength calibration. We use the *Austral* code (Endl et al. 2000) for the computation of precise differential radial velocities.

The scatter of the HIRES observations is 4.4 m s$^{-1}$, which is higher than our 2.8 m s$^{-1}$ median error bar. The difference amounts to 3.4 m s$^{-1}$ and can be explained by typical jitter values as measured in other stars. For example, Wright (2005) finds a median stellar jitter of $\sigma'_{RV} = 4.4$ m s$^{-1}$ for inactive stars

---

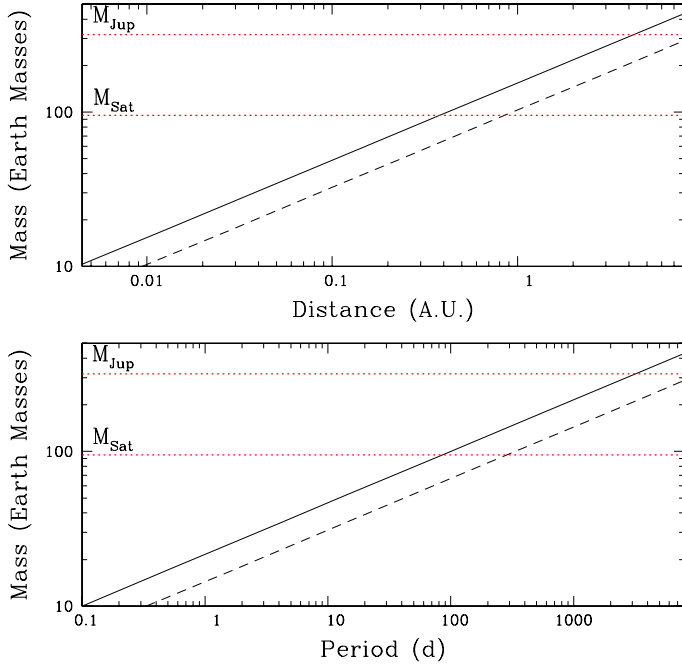[5] The HIRES data for HIP 56948 were obtained at times when the CoRoT field was unobservable.

**Fig. 3.** Estimated sensitivity of our observations as a function of distance (*upper panel*) and orbital period (*lower panel*). The 2-$\sigma$ and 3-$\sigma$ sensitivities are shown by dashed and solid lines, respectively. The red dotted lines represent planets with 1 $M_{Jup}$ and 1 $M_{Sat}$. Our radial velocity data discard planets as massive as Jupiter in the terrestrial planet region.

with $(B - V) > 0.60$. Interestingly, the McDonald observations seem to be less affected by stellar jitter, due to the much longer exposure times required when compared to the Keck observations (~3 min), damping the radial velocity variations due to stellar jitter. Indeed, one of the observational strategies to reduce stellar noise in short time scales (mainly stellar oscillations) is to take relatively long exposures (e.g. a long 10-min exposure, or the average of several short exposures), thus improving the precision of the observations (Dumusque et al. 2011). We verified this with our Keck data taken during four nights in January 2012. Each night we took three consecutive short (~3 min) exposures, so that the average exposure for a given night has a much lower contribution from stellar noise (lower panel of Fig. 2). The night-to-night scatter is only 3.3 m s$^{-1}$, in reasonable agreement with our observational error bar of 2.8 m s$^{-1}$. The Keck measurements taken in February 2011 and in January−February 2012 clearly rule out hot Jupiters, and we can even eliminate the presence of planets with masses as low as Neptune in the inner 0.04 AU (lower panel of Fig. 2).

Considering that velocity semi-amplitudes about 2–3 times the typical measurement precision (in our case ~4 m s$^{-1}$) can be detected with confidence, we can rule out the presence of a stellar companion and nearby giant planets. As shown in Fig. 3, where the 2-$\sigma$ (dashed line) and 3-$\sigma$ (solid line) sensitivity of our observations are shown (computed as the planetary mass that would introduce detectable radial velocity variations), there is no indication of a Jupiter-mass planet in the terrestrial planet region (<3 AU), and even a less massive giant planet such as Saturn may be ruled out (at the 2-$\sigma$ level) inside 1 AU So, the inner region around HIP 56948 seems free from giant planets. Examples of some circular orbits for a Jupiter-mass planet at 1 AU (Earth's distance from the Sun), 1.5 AU (Mars' distance from the Sun) and 3 AU, are shown in the upper panel of Fig. 2. We have

verified for a range of planetary masses, distances, random observing times and including error bars in the measurements, that no giant planet is present, although notice that since our data are sparsely sampled, some giant planets (especially on orbits with $e > 0$) may have escaped detection. Once more radial velocity data are obtained in the coming years we intend to perform detailed simulations to see which kind of planets we could have missed. With the existing dataset, we see no evidence of giant planets in the inner region around HIP 56948.

Provided we maintain a radial velocity precision of about 4–5 m s$^{-1}$ for our observations, in a decade or so we should be able to detect (or rule out) the presence of a Jupiter twin, i.e., a Jupiter-mass planet orbiting at 5 AU from HIP 56948.

We will discuss the implications of the constraints we have deduced which limit the presence of massive planets in the inner regions around HIP 56948 further in Sect. 4, in combination with our findings of the chemical similarities between HIP 56948 and the Sun.

## 3. Abundance analysis

The abundance analysis is based on the Keck HIRES spectra, following our previous differential work on solar twins (Meléndez et al. 2006; Meléndez & Ramírez 2007; Meléndez et al. 2009; Ramírez et al. 2009), where the solar and stellar spectra are measured in exactly the same way.

An initial set of equivalent width (EW) measurements was obtained by fitting Gaussian profiles with the automatic routine ARES (Sousa et al. 2007). We computed the relative difference in equivalent width between HIP 56948 and the Sun, $\delta W_r = (EW^* - EW^\odot)/EW^\odot$, and lines with $\delta W_r$ deviating from the median $\langle \delta W_r \rangle$ for a given species, were measured by hand both in HIP 56948 and the Sun. All weak lines ($EW < 10$ mÅ) and the lines of species with only a few lines available, were also measured by hand. About 20% of the EW measurements needed to be checked according to our initial empirical analysis, although note that this procedure only reveals the most obvious outliers. The deviating automatic ARES measurements could be due to any of these causes: *i)* the number of components found by ARES in the local fitting window is not exactly the same in the spectrum of HIP 56948 and the Sun, *ii)* the 2nd-order polynomial used to fit the local continuum could be somewhat different in both stars, *iii)* contamination by telluric lines do not fall exactly on the same place in both stars. Indeed, most faulty automatic measurements occur either in the blue, where the spectrum is more crowded, or in the red, where telluric contamination is higher.

An initial model atmosphere analysis was performed using the improved EW measurements and again we look for outliers from the mean abundance for each species, and they are checked by hand. In most cases the revised measurements result in a reduced scatter. The improved EW is mainly due to more consistent manual measurements, which are performed using exactly the same continuum for the Sun and the twin, and also the same part of the profile, or the same treatment of blends. This is not always the case with the automatic ARES measurements. The final analysis is performed using the set of revised equivalent widths, except for lithium which is analyzed using spectral synthesis. The adopted EW for HIP 56948 and the Sun are given in Table 3.

We use 1D Kurucz overshooting model atmospheres (Castelli et al. 1997), as well as MAFAGS-OS (Grupp 2004) and MARCS (Gustafsson et al. 2008) 1D LTE (local thermodynamic

equilibrium) models. The models have different mixing-length approaches, as explained in detail in the above references. The differences in stellar parameters, between HIP 56948 and the Sun, are small, therefore essentially the same results (within ~0.001 dex) are obtained with either Kurucz or MAFAGS-OS models.

The analysis has been performed both in LTE and NLTE (non-LTE). For the LTE calculations we used the 2002 version of MOOG (Sneden 1973), while the NLTE calculations are described in Sect. 3.3.

### 3.1. Stellar parameters

The stellar parameters adopted for the Sun are $T_{\rm eff}$ = 5777 K and $\log g$ = 4.44 (e.g. Cox 2000). With $T_{\rm eff}$ and $\log g$ set, the microturbulence velocity ($v_t$) is found by requiring no dependence of $A(\rm Fe)$[6] with reduced equivalent width $EW_r$ (=EW/$\lambda$) for FeI lines. We found $v_{\rm t}^{\odot}$ = 0.99 km s$^{-1}$ both for Kurucz and MAFAGS models. The above set of parameters (5777 K, 4.44 dex, 0.99 km s$^{-1}$) yielded the zero-point solar abundances for each line $i$, $A_i^{\odot}$ for a given model atmosphere.

For HIP 56948, an initial set of stellar parameters was found in LTE using Kurucz models. The *relative* spectroscopic equilibrium was achieved using differential abundances $\delta A_i$ for each line $i$,

$$\delta A_i = A_i^* - A_i^{\odot}. \tag{1}$$

Thus, the effective temperature is found by imposing the relative excitation equilibrium of $\delta A_i$ for FeI lines:

$$d(\delta A_i^{\rm FeI})/d(\chi_{\rm exc}) = 0, \tag{2}$$

while the surface gravity ($\log g$) is obtained using the relative ionization equilibrium. Usually, this is done using FeI and FeII, but in our case we verified that within the error bars the ionization balance is fulfilled simultaneously for Fe, Ti and Cr. Therefore, we use the mean relative ionization equilibrium between FeI and FeII, TiI and TiII, and CrI and CrII:

$$\Delta^{\rm FeII-FeI} \equiv \langle \delta A_i^{\rm FeII} \rangle - \langle \delta A_i^{\rm FeI} \rangle$$

$$\Delta^{\rm TiII-TiI} \equiv \langle \delta A_i^{\rm TiII} \rangle - \langle \delta A_i^{\rm TiI} \rangle$$

$$\Delta^{\rm CrII-CrI} \equiv \langle \delta A_i^{\rm CrII} \rangle - \langle \delta A_i^{\rm CrI} \rangle$$

$$\Delta^{\rm II-I} \equiv (3\Delta^{\rm FeII-FeI} + 2\Delta^{\rm TiII-TiI} + \Delta^{\rm CrII-CrI})/6 = 0, \tag{3}$$

with the weights arbitrarily chosen, but reflecting increasingly larger errors for FeI/FeII, TiI/TiII and CrI/CrII.

The microturbulence velocity $v_t$ was obtained when the differential abundances $\delta A_i^{\rm FeI}$ showed no dependence with reduced equivalent width $EW_r$:

$$d(\delta A_i^{\rm FeI})/d(EW_r) = 0. \tag{4}$$

The spectroscopic solution is found when the three conditions above (Eqs. (2)–(4)) are satisfied simultaneously, and when the metallicity obtained from the iron lines is the same as that of the input model atmosphere. Notice from the equations above that our work is strictly differential, i.e., we do not enforce absolute spectroscopic equilibrium, which may be difficult to achieve (both in LTE and NLTE) even in the Sun (Mashonkina et al. 2011; Bergemann et al. 2012).

---
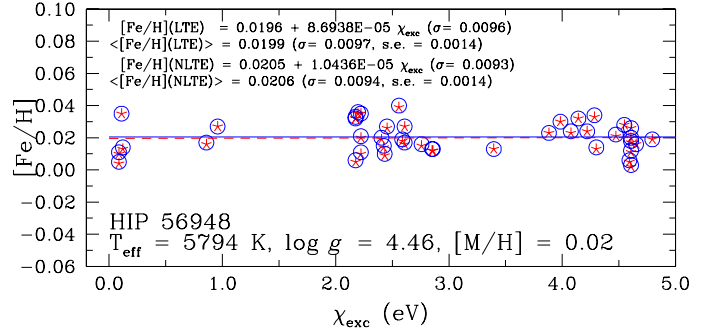[6] $A(\rm X) \equiv \log(N_{\rm X}/N_{\rm H}) + 12$.



**Fig. 4.** Iron abundances versus excitation potential of FeI lines in LTE (red stars) and NLTE (blue circles). The blue solid and the red dashed lines show the fit in NLTE and LTE, respectively. The line-to-line scatter in NLTE is only $\sigma = 0.009$ dex and the standard error is 0.001 dex.

The initial LTE solution with Kurucz models showed that indeed HIP 56948 is extremely similar to the Sun, with differences (HIP 56948 − Sun) in $T_{\rm eff}/\log g/$[Fe/H]$/v_t$ of only 17 K/0.02 dex/0.02 dex/0.01 km s$^{-1}$. We also tried the MAFAGS-OS models and the same stellar parameters were obtained, with a negligible difference of ±0.001 dex in [Fe/H] from FeI and FeII lines with respect to the Kurucz models, and with a difference in the spectroscopic $T_{\rm eff}$ of only 0.1 K.

Given the very similar stellar parameters between HIP 56948 and the Sun, we do not anticipate NLTE considerations to produce significant changes to the stellar parameters. Indeed, the NLTE Fe abundances indicate the same $T_{\rm eff}$ within 0.4 K, with the LTE temperature being slightly cooler. In Fig. 4 we show the individual iron abundances as a function of excitation potential of the FeI lines, both in LTE and NLTE. The NLTE abundances result in ever so slightly lower line-to-line scatter ($\sigma = 0.009$ dex, s.e. = 0.001 dex) than in LTE.

Unfortunately the trigonometric Hipparcos parallax for HIP 56948 is not known with enough precision to provide better constraints than our spectroscopic value. The Hipparcos value is $\log g = 4.37 \pm 0.07$ (Table 4), which agrees within 1-$\sigma$ with our result from spectroscopy ($\log g = 4.46 \pm 0.02$). The above error in the trigonometric $\log g$ is due to both the uncertainty in the Hipparcos parallax and typical errors in photometric temperatures (e.g. Meléndez et al. 2010b). Adopting instead our more precise stellar parameters we obtain a Hipparcos-based gravity of $\log g = 4.37 \pm 0.05$, which agrees with our spectroscopic gravity within 1.3-$\sigma$.

Notice that the Hipparcos parallax ($15.68 \pm 0.67$ mas, according to the new data reduction by van Leeuwen 2007) implies a distance of $63.8 \pm 2.7$ pc for HIP 56948. We can obtain an independent estimate of this distance assuming that the absolute magnitude of HIP 56948 is identical to solar; i.e. $M_{\rm V} = 4.81$ (Bessell et al. 1998). Since $V = 8.671 \pm 0.004$ and the error in the absolute magnitude from the uncertainty in our stellar parameters is 0.055 mag (see Eq. (8)), we derive a distance of $59.2 \pm 1.5$ pc. Thus, there is agreement within 1.1$\sigma$ for both distance estimates.

The adopted stellar parameters, errors, and comparison with other estimates, are given in Table 4. Overall there is a good agreement (within the error bars) with other independent estimates. The errors depend on the quality of the spectra of both HIP 56948 and the Sun. Since the S/N is very high ($\gtrsim 600$) we can put stringent constraints on the stellar parameters. Nevertheless, we are also limited by the degeneracy between $T_{\rm eff}$, $\log g$, [Fe/H] and $v_t$, which increases the errors.

As described in Appendix C, for a fixed $\log g$ (or a small range of $\log g$ values), we could determine $T_{\text{eff}}$ to within 0.8 K, while if $T_{\text{eff}}$ is keep fixed (or within a small range), $\log g$ could be determined to within 0.006 dex. Regarding the microturbulence, for a fixed $T_{\text{eff}}$ and $\log g$, $v_t$ could be determined to within 0.0004 km s$^{-1}$. Due to the degeneracies between stellar parameters and to the observational uncertainties, the errors are actually considerably larger (Table 4), 7 K, 0.02 dex and 0.01 km s$^{-1}$ for $T_{\text{eff}}$, $\log g$ and $v_t$, respectively. A detailed description of the determination of stellar parameters and the uniqueness of our solution is given in Appendix C.

As a further check of the effective temperature, we have tried to compare synthetic H$\alpha$ profiles, computed using MAFAGS-OS models, to the observed H$\alpha$ profiles in HIP 56948 and the Sun. Unfortunately H$\alpha$ falls on an order too close to the edge of the chip, making it difficult to normalize that region properly. Despite the above problem, our tests using H$\alpha$ indicate that indeed HIP 56948 is somewhat hotter ($\sim +20 \pm 20$ K) than the Sun, in agreement with what is found from iron lines.

### 3.2. LTE abundances

The adopted atomic data is presented in Table 3. Whenever possible we use laboratory oscillator strengths, or theoretical $gf$-values normalized to laboratory data (e.g., Fuhr & Wiese 2006; Meléndez & Barbuy 2009). However, the input $gf$-values are not critical, as they cancel out in the line-by-line differential abundances $\delta A_i$. The interaction constants $C_6$ were computed from the broadening cross-sections calculated by Barklem et al. (2000) and Barklem & Aspelund-Johansson (2005), using the transformation given in Meléndez & Barbuy (2009). If broadening cross-sections were not available, we multiply the classical Ünsold constant by 2.8. The adopted $C_6$ values are given in Table 3.

The mean $\langle \delta A_i \rangle$ and the standard deviation are computed for each atomic species, so that we readily identify any outliers. The suspicious measurements are checked by hand, both in the Sun and HIP 56948, using insofar as possible the same measurement criteria, i.e., the same continuum regions are adopted and exactly the same part of the line profile is used for the Gaussian fit.

Equivalent widths were used to obtain abundances for all elements except for lithium, which was analyzed using spectrum synthesis, as in our previous work on solar twins (Meléndez et al. 2006; Meléndez & Ramírez 2007; Baumann et al. 2010). The line list used for spectral synthesis is presented in Table 5. The data for the Li doublet was taken from the laboratory data presented in Andersen et al. (1984). Although Smith et al. (1998) and Hobbs et al. (1999) reported new $gf$-values based on theoretical calculations, the difference with our adopted laboratory values is only ~1%. Other atomic lines near the Li feature were taken from Mandell et al. (2004) and the Kurucz[7] and VALD (Kupka et al. 2000) databases, adjusting in some cases their $gf$-values to better reproduce the solar spectrum. Molecular lines of CN (Meléndez & Barbuy 1999; Mandell et al. 2004) and C$_2$ (Meléndez & Cohen 2007; Meléndez & Asplund 2008) were also included in the spectral synthesis.

The LTE abundances were computed using Kurucz models and checked using MAFAGS-OS models. The agreement is excellent, with a mean difference (MAFAGS − Kurucz) of only −0.0010 dex in the differential abundances, and with a element-to-element scatter in the differential abundances of only

0.00075 dex (0.17%), which is quite remarkable and shows the weak dependence of our strict differential analysis to the adopted model atmosphere[8].

The LTE differential abundances are provided in Table 6, but note that the adopted abundances are those based on NLTE (when available). The observational errors, which depend mainly of the quality (S/N) of the spectra of both HIP 56948 and the Sun, are given also in Table 6. The observational error is adopted as the standard error ($=\sigma/\sqrt{n}$) when more than three lines of a given species are available. Otherwise we assumed a minimum value of $\sigma_{\text{min}} = 0.009$ dex (s.e. = 0.005 dex for 3 lines; s.e. = 0.006 dex for 2 lines), which is the typical line-to-line scatter for species with more than 10 lines available. When only 2 or 3 lines were available we adopted the maximum value of the observed $\sigma$ and $\sigma_{\text{min}}$, i.e., max($\sigma$, 0.009 dex). If only one line was available, we estimated the error by performing a number of measurements with different assumptions for continuum placement (within the noise of the spectra) and profile fitting.

In addition to the observational errors, we also present the errors due to uncertainties in the stellar parameters in Table 6, where the total error is also given. As shown in Appendix B, our very small observational errors ($\sim 0.005$ dex) are plausible.

### 3.3. NLTE abundances

For most of the elements we have been able to account for departures from local thermodynamic equilibrium (NLTE). For Li, C, O and Na we have employed MARCS model atmospheres (Gustafsson et al. 2008) and the model atoms described in Lind et al. (2009), Fabbian et al. (2006, 2009) and Lind et al. (2011a), respectively, using up-to-date radiative and collisional data. We note that for Li and Na, quantum mechanical estimates of the cross-sections for collisions with both electrons and hydrogen are available. For O we adopt a scaling factor $S_H$ of 0.85 to the classical formula of Drawin (1968, 1969) for excitation and ionization due to inelastic H collisions as empirically determined from the solar center-to-limb variation by Pereira et al. (2009). For C we adopt $S_H = 0.1$ in the absence of similar empirical evidence. For these elements the NLTE calculations were performed with the 1D statistical equilibrium code MULTI (Carlsson 1986).

In addition, we performed NLTE calculations for Mg, Al, Ti, Cr, Mn, Fe, Co, and Ba, using the revised version of the DETAIL code (originally published in Giddings 1981) and the SIU code (Reetz, unpublished). We used MAFAGS-OS 1D LTE model atmospheres (Grupp 2004) provided by F. Grupp (priv. comm.). The differences in abundances required to equalize NLTE and LTE equivalent widths are defined as NLTE corrections.

For Mg and Al, the model atoms were kindly provided by Gehren; those models were previously used in the spectroscopic analysis of solar-type stars given in Gehren et al. (2004, 2006). Atomic models for Cr, Mn, Co, and Ti, were taken from Bergemann & Cescutti (2010), Bergemann & Gehren (2008), Bergemann et al. (2010), and Bergemann (2011), respectively. To compute NLTE corrections for the lines of Fe I/II, and Ba II, we constructed the model atoms from the laboratory and

---

[7] http://kurucz.harvard.edu/

[8] The MARCS model and the mean atmospheric structure of a 3D model atmosphere (Asplund et al. 2009), are much closer to the MAFAGS-OS model than to the Kurucz overshooting model, thus the effects of using either the MARCS or the 3D model would be even smaller than for the comparison between MAFAGS-OS and Kurucz overshooting models.

theoretical data given in NIST[9] and Kurucz[10] databases. For Fe I, we also used highly-excited predicted levels and transitions as recommended by Mashonkina et al. (2010), who showed that the inclusion of these data is necessary for a realistic representation of statistical equilibrium of Fe in the atmospheres of cool stars. Photoionization cross-sections for Fe I levels were taken from Bautista (1997). The detailed description of the Fe model is given in Bergemann et al. (2012).

A critical parameter in the statistical equilibrium calculations is the efficiency of inelastic collisions with H I. In the absence of quantum-mechanical data, we computed the cross-sections for excitation and ionization by H I atoms from the formulae of Drawin (1969). Following the above-mentioned studies, we adopted individual scaling factors $S_H$ to the Drawin-type cross-sections for each element: Mg (0.05), Al (0.002), Ti (0.05), Cr (0), Mn (0.05), Co (0.05). These scaling factors were determined by requiring consistent ionization-excitation equilibria of the elements under restriction of different stellar parameters. For Fe and Ba, we used $S_H = 0.1$, and 0.05, respectively.

We performed another set of independent non-LTE calculations for Na using MAFAGS-OS models and the model atom described by Gehren et al. (2006), but the mean Na abundance only changes by 0.001 dex with respect to the value obtained using the most up-to-date model atom by Lind et al. (2011a).

Besides the elements above (Li, C, O, Na, Mg, Al, Ti, Cr, Mn, Fe, Co, and Ba) for which specific NLTE calculations were performed for the present work, we estimate NLTE corrections for K, Ca, Zn and Zr, using the grid of NLTE corrections computed by Takeda et al. (2002), Mashonkina et al. (2007), Takeda et al. (2005) and Velichko et al. (2010), respectively. Nevertheless, the differential NLTE abundance corrections are negligible for these elements (≤0.001 dex).

All the differential NLTE corrections (HIP 56948 – Sun) are given in Table 3, except for Li. For this element the differential NLTE correction amounts to only −0.001 dex and the adopted differential NLTE Li abundance is given in Table 4.

### 3.4. The abundance pattern of HIP 56948

In Fig. 5 we plot the differential abundances [X/H] between HIP 56948 and the Sun (circles) as a function of equilibrium condensation temperature ($T_{cond}$, Lodders 2003). The fit of [X/H] vs. $T_{cond}$ is shown for volatile ($T_{cond} < 1000$ K) and refractory ($T_{cond} > 1000$ K) elements[11]. As can be seen, the element-to-element scatter around the fit is extremely small, only 0.004 dex for the volatiles and 0.007 dex for the refractories. Both are of the same order as the observational error bars, which are $\sigma_m(obs) \sim 0.006$ dex for volatiles and $\sigma_m(obs) \sim 0.004$ dex for refractories, hence showing that it is possible to achieve abundances with errors as low as ~0.005 dex. If we take into account the errors due to uncertainties in the stellar parameters (Table 6), then the expected total median errors (including
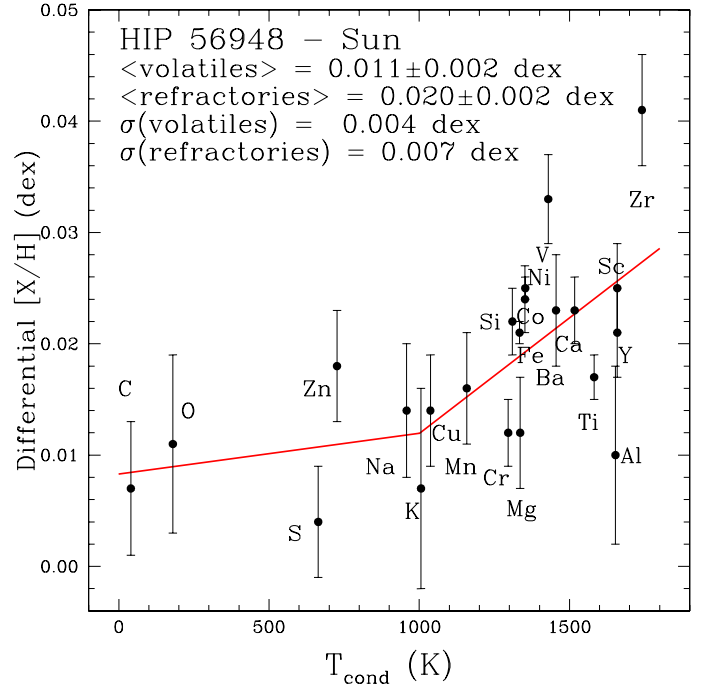
---

[9] http://www.nist.gov/physlab/data/asd.cfm

[10] http://kurucz.harvard.edu/

[11] Notice that for the abundance pattern of HIP 56948 the best fit is found for a break at $T_{cond} = 1000$ K, while for the average of solar twins the break is at $T_{cond} = 1200$ K. Although the break point was determined by fitting independently the refractory and volatile elements, and choosing the break by minimizing the scatter in both sides, with minor adjustments to provide the best match at the break point, our results are confirmed by a global fitting that assumes two linear functions to fit the whole dataset by assuming that those functions are equal at the break point.



**Fig. 5.** Abundance pattern of HIP 56948 (circles) versus condensation temperature. The solid line represents the mean abundance pattern. The error bars are based only on the observational uncertainties, which are ~0.005 dex. The low element-to-element scatter from the fit for the volatile ($\sigma = 0.004$ dex) and refractory ($\sigma = 0.007$ dex) elements confirms the high precision of our work.

observational errors) are 0.007 dex for volatiles and 0.008 dex for refractories, i.e., somewhat higher than the observed scatter (0.004 and 0.007 dex, respectively) around the mean trends. That means that we may be slightly overestimating our errors, and that a more representative total error for our abundances is ~0.006 dex. As can be seen in Table 6, it is possible to obtain a total error as small as 0.004 dex (Si) or 0.005 dex (Ni), and for several elements errors as small as 0.006 dex can be achieved (Ca, Cr, Fe, Co, Zn).

The mean [X/H] ratio of the volatile and refractory elements is ⟨[volatiles/H]⟩ = 0.011 (s.e. = 0.002) and ⟨[refractories/H]⟩ = 0.020 (s.e. = 0.002), respectively. Thus, the mean difference between refractories and volatiles in HIP 56948 amounts to only 0.009 dex, i.e., HIP 56948 has an abundance pattern very similar to solar.

In Fig. 6 we plot the differential abundances [X/⟨C, O⟩] between HIP 56948 and the Sun (circles) as a function of condensation temperature. Here the average of carbon and oxygen, ⟨C, O⟩, is chosen as the reference, as those elements should not be depleted in the solar atmosphere (Meléndez et al. 2009). We also show with a solid line the mean[12] abundance pattern of the 11 solar twins studied by Meléndez et al. (2009). The dashed line represents the mean behavior of HIP 56948 shown in Fig. 5. This figure shows clearly that the abundance pattern of HIP 56948 is much closer to the Sun than to the mean abundance pattern of other solar twins.

The volatile elements with $T_{cond} < 1000$ K have a similar behavior in HIP 56948 and the Sun, while the refractory elements are depleted (with respect to other solar twins) both in HIP 56948 and the Sun, although they are somewhat less

---

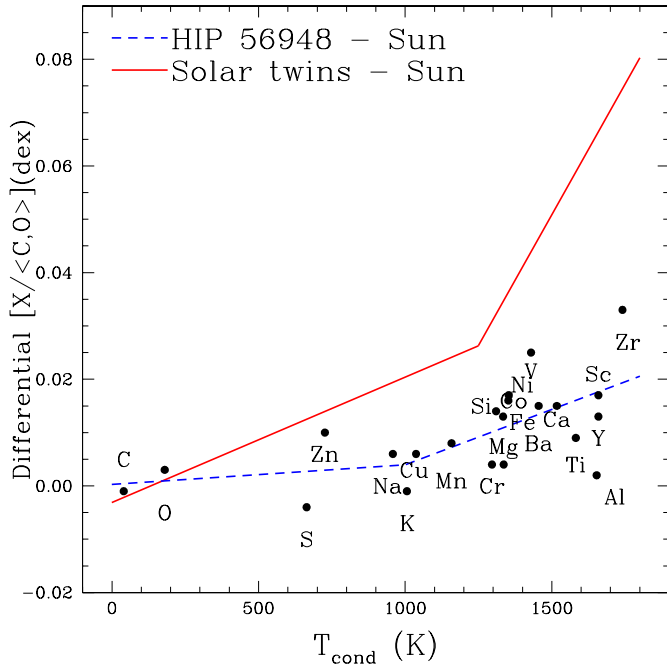[12] The robust estimator *trimean* is used.

**Fig. 6.** Abundance pattern of HIP 56948 (circles) versus condensation temperature. The average of the highly volatile (low $T_{cond}$) elements C and O is used as reference. The solid line represents the mean abundance pattern of the 11 solar twins studied by Meléndez et al. (2009) and the dashed line represents the fit to the abundance pattern of HIP 56948. Clearly, HIP 56948 is much closer to the Sun than to other solar twins.

depleted (by ~0.01 dex) in HIP 56948. Therefore, it seems that somewhat less dust was formed around HIP 56948 than around the Sun. Interestingly, in the sample of solar twins studied so far, the Sun seems to be the most depleted in refractories. If this peculiar abundance pattern is related to the formation of rocky planets (Meléndez et al. 2009; Ramírez et al. 2009, 2010; Chambers 2010), that signature could be used to search for possible candidates to host terrestrial planets. Below, we discuss in detail various other possibilities that could cause abundance anomalies.

## 4. Discussion

From the determination of isotopic abundances in meteorites it has been shown that short-lived radionuclides were present in the early stages of the solar system, perhaps due to pollution by an asymptotic giant branch (AGB) star (Wasserburg et al. 1994; Busso et al. 1999; Trigo-Rodríguez et al. 2009) or by supernova (Cameron & Truran 1977; Boss & Foster 1998; Ouellette et al. 2010), although other causes may be possible. Thus, before discussing the terrestrial planet formation scenario, we assess if the solar anomalies may be due to other causes such as pollution by intermediate or high mass stars.

### 4.1. Abundance anomalies: AGB/SN pollution or terrestrial planets?

In Meléndez et al. (2009) we argued against the hypothesis that the abundance anomalies found in the Sun could be due to galactic chemical evolution effects or supernova pollution, as the solar chemical peculiarities do not seem to follow those abundance

patterns. Here, we study in more detail whether the anomalies could be due to pollution by an AGB star, thermo-nuclear supernovae (SNIa), core-collapse supernovae (SNII) or a hypernova (HN), by subtracting the yields of those objects from the solar nebula (i.e., "de-polluting" the solar abundances) and comparing the results to the pattern of the solar twins.

Following the tentative AGB pollution scenario of Trigo-Rodríguez et al. (2009), we use a dilution factor of 1 part of AGB material per 300 parts of original solar nebula material (equivalent to mixing 0.0185 $M_{\odot}$ of AGB ejecta), for which solar abundances from Anders & Grevesse (1989) were adopted. Note that the use of the new solar abundances by Asplund et al. (2009) do not have a significant impact on the abundance trend, as shown in Fig. 7 (top panel). For SNIa, SNII, and HN we assume that the same amount of mass as used in the AGB scenario is mixed into 1 $M_{\odot}$ of solar system material. For consistency with the AGB scenario we use the solar abundances from Anders & Grevesse (1989).

The amount of material that would actually be injected is uncertain. There is no reason that a SN would inject about the same amount of mass as an AGB star. Young et al. (2011) note that SN are more likely to pollute the entire molecular star forming cloud, not an individual protosolar nebula. They estimate that a ~1% enrichment of the protosolar molecular cloud by ejecta from SNII can account for the oxygen isotope ratios measured in the solar system. However as we are only interested in the qualitative impact (trend with condensation temperature) that such yields have on a protosolar nebula and not the quantitative details, the actual amount of pollution from an individual SN or AGB model should not strongly impact our conclusions. The same can be said for the exact amount of the AGB and SN yields, which are inherently quite uncertain.

A massive AGB star of 6.5 $M_{\odot}$ was chosen, as it has a short lifetime (~55 Myr). Our AGB model and yields are described in Karakas & Lattanzio (2007), Trigo-Rodríguez et al. (2009) and Karakas (2010). The results after removing the AGB pollution are shown in Fig. 7 (top panel). As can be seen, contamination by a massive AGB star cannot explain the abundance trend with $T_{cond}$. The main signature from an hypothetical 6.5-$M_{\odot}$ AGB star would be a large change in nitrogen.

We have also considered pollution by SNII, HN, and SNIa, according to the yields described in Kobayashi et al. (2006), Kobayashi & Nomoto (2009) and Kobayashi & Nakasato (2011). Miki et al. (2007) suggest that a supernova of a massive star of at least 20 $M_{\odot}$ was responsible for the anomalies of short-lived radionuclides discussed above, so for the SNII and HN, a 25 $M_{\odot}$ was adopted. As seen in Fig. 7, the trend with condensation temperature cannot be explained by either SNII or HN.

Finally, for the binary system leading to a SNIa, we choose a system composed of a 3 $M_{\odot}$ of primary star + 1.3 $M_{\odot}$ of secondary star, with a metallicity of 0.1 $Z_{\odot}$ for the progenitors, which are supposed to have been born 4.5 Gyr ago. The binary system evolves to ~1 $M_{\odot}$ C+O white dwarf plus 1.3 $M_{\odot}$ of secondary star, then to 1.374 $M_{\odot}$ SNIa + 0.9 $M_{\odot}$ remnant of the secondary star. Thus, for the contamination by ejecta of SNIa, we include 1.374 $M_{\odot}$ of processed metals by SNIa plus $(3 + 1.3 - 0.9 - 1.374)$ $M_{\odot}$ of unprocessed matter in the stellar winds.

Again, pollution by SNIa cannot explain the peculiar solar abundance pattern (Fig. 7). We also tried other combinations for the progenitors of SNIa, but these yields also do not reproduce the trend with condensation temperature shown in Fig. 7.
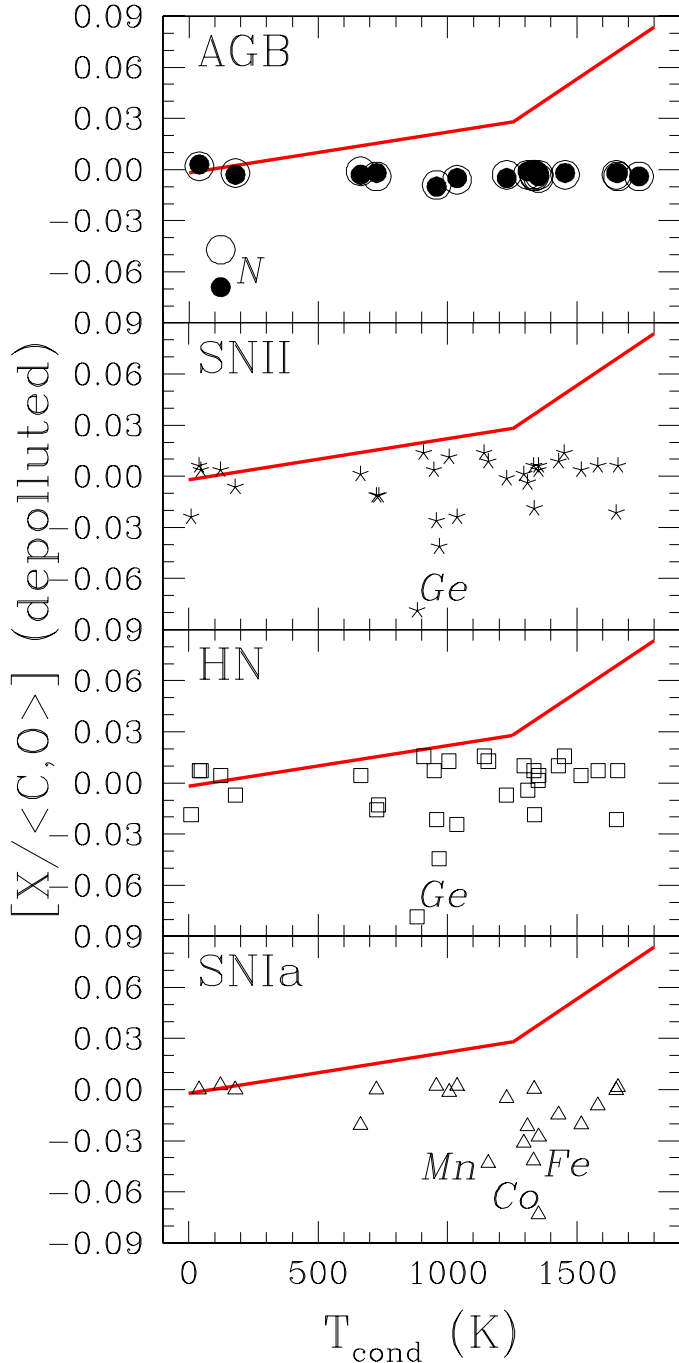
**Fig. 7.** Abundance ratios obtained after de-polluting the solar nebula from contamination by an AGB star (circles), SNII (stars), hypernova (squares) and SNIa (triangles). In the top panel the effect of adopting different solar abundances (open circles: Anders & Grevesse 1989; filled circles: Asplund et al. 2009) is shown. The solid line represents the mean abundance pattern of 11 solar twins relative to the Sun (Meléndez et al. 2009). None of the pollution scenarios can explain the trend with condensation temperature. For clarity, the abundance ratios of SNII, HN and SNIa have been divided by 4, 3.5 and 14, respectively. The chemical elements that change the most are labeled.

**Fig. 8.** Composition of the solar twins with respect to HIP 56948 (dashed line) and the Sun (solid line). The open circles show the effect of adding 6 $M_\oplus$ of a mix of Earth-like and meteoritic-like material (Chambers 2010) to the convection zone of the present Sun (Asplund et al. 2009), and the filled circles the effect of adding 3 $M_\oplus$ of rocky material to the convection zone of HIP 56948. Abundances are normalized with respect to $\langle$C, O$\rangle$. Both the Sun and HIP 56948 require $\sim$2 $M_\oplus$ of Earth-like material, while the Sun requires much larger quantities of chondrite material. Notice the very small (<0.01 dex) element-to-element scatter.

Therefore, we conclude that the peculiar solar abundance pattern cannot be due to contamination by AGB stars, SNIa, SNII or HN, as predicted by state-of-the-art nucleosynthesis models. We emphasize that our results do not rule out that a SN or AGB star contaminate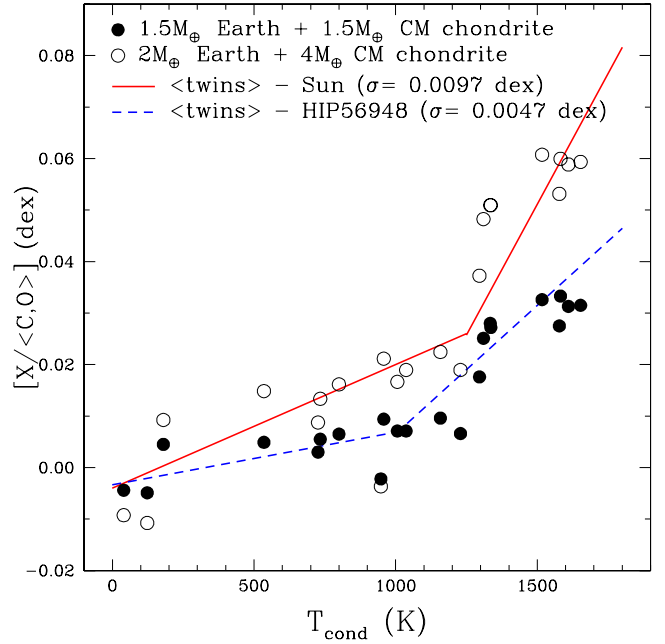d the proto-solar nebula to cause the observed isotopic anomalies in meteorites, rather, we discard pollution as a viable explanation of the peculiar elemental abundances in the Sun.

### 4.2. The abundance pattern of HIP 56948 and terrestrial planets

As discussed above, pollution from stellar ejecta cannot explain the anomalous solar abundance pattern. A possible explanation for the peculiarities is the formation of terrestrial planets (Meléndez et al. 2009; Ramírez et al. 2009, 2010; Gustafsson et al. 2010; Chambers 2010). The same planet formation scenario may be applied to HIP 56948. To verify this, we obtained the abundance ratios of the 11 solar twins of Meléndez et al. (2009) relative to HIP 56948, again using the average of C and O as reference. The resulting mean trend is represented by a dashed line in Fig. 8. The trend of solar twins relative to the Sun is shown by a solid line.

Thus, the same terrestrial planet formation scenario could be applied to HIP 56948, except that the Sun has ∼0.01 dex smaller refractory-to-volatile ratio than HIP 56948. So, the Sun could have formed more rocky planets than HIP 56948, or perhaps slightly more massive rocky planets than in HIP 56948. In any case, the overall amount of rocky material may have been higher around the Sun than around HIP 56948.

Recently, Chambers (2010) has shown that a mix of 4 Earth masses of Earth-like and meteoritic-like material, provides an excellent element-to-element fit for the solar abundance

anomalies for about two dozen chemical elements[13]. Interestingly, the above mixture reproduces the anomalies significantly better than a composition based either only on Earth material or only on carbonaceous-chondrite meteorites. Using his detailed abundance pattern of Earth and carbonaceous chondrites, we can check whether the same mixture could fit HIP 56948. Indeed, as shown in Fig. 8, a 3-Earth-mass mixture of Earth plus meteorites (filled circles) provides an excellent fit to the abundance pattern of the solar twins relative to HIP 56948 (dashed line). The element-to-element scatter of the Earth/chondrite mix with respect to the fit (dashed line) is only 0.005 dex. Notice that the chemical elements included in Fig. 8 are not necessarily the same ones studied in HIP 56948 because for the Earth/meteoritic mix we can include other elements such as fluorine and uranium (Chambers 2010).

The abundance pattern of the solar twins with respect to the Sun (Fig. 8, solid line), seems to require more than the four Earth masses suggested by Chambers (2010). Note that we are normalizing to $\langle C, O \rangle$, while Chambers (2010) normalizes to iron, and that the mean solar abundance trend adopted by Chambers (2010) may be slightly different than ours, hence some differences are expected. The fit for the Sun ($\sigma = 0.010$ dex) is not as good as for HIP 56948 ($\sigma = 0.005$ dex). In total 6 $M_\oplus$ of rocky material is needed to fit the Sun, while 3 $M_\oplus$ is needed to fit HIP 56948. So, perhaps about twice more rocky material was formed around the Sun than around HIP 56948.

Interestingly, both the Sun and HIP 56948 seem to require about the same mass of Earth-like material (2 and 1.5 $M_\oplus$, respectively), but the amount of CM chondrite material seems much higher for the Sun (4 $M_\oplus$) than for HIP 56948 (1.5 $M_\oplus$). Although 4 Earth masses of meteoritic material may seem too high considering the current mass of the asteroid belt, various models predict that the belt has lost most of its mass (e.g., Weidenschilling 1977; Wetherill 1989, 1992; Petit et al. 1999; Chambers & Wetherill 2001; Minton & Malhotra 2010). In particular, the simulations by Chambers & Wetherill (2001) show that a few Earth masses of material from the belt can be removed, either via collisions with the Sun or ejected from the solar system. In contrast, material in the terrestrial-planet region had a good chance of surviving (Chambers & Wetherill 2001). Thus, albeit a large mass of material may have formed in the asteroid belt, most of the initial mass has already been removed.

The 2 $M_\oplus$ of Earth-like material seen in the chemical composition of the Sun is comparable with the total mass of the terrestrial planets in the solar system, and only somewhat higher than the amount of Earth-like material around HIP 56948. As shown above, the different slopes of the abundances of volatile and refractory elements (with condensation temperature) may be used to constrain the type of solid bodies that were originated as a result of planet formation using the different abundance patterns of the Earth and meteorites (Chambers 2010). Thus, the careful analysis of stellar chemical compositions offer the thrilling prospect of determining which type of rocky objects were formed around stars.

In line with our above findings on the similarities between HIP 56948 and the Sun, the radial velocity monitoring of HIP 56948 (Sect. 2.2) shows no indication of inner (<3 AU) giant planets, as massive as Saturn or Jupiter. Thus, the inner
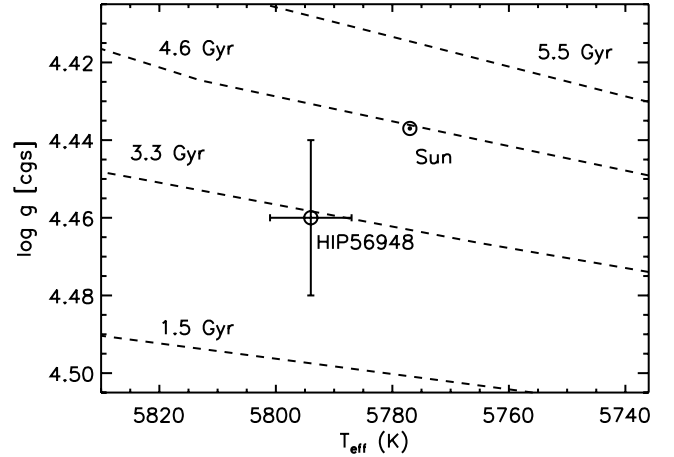


**Fig. 9.** Location of the Sun and HIP 56948 on the HR diagram. Note the very small range of stellar parameters. Solar-metallicity isochrones of 1.5, 3.3, 4.6, and 5.5 Gyr are shown (dotted lines). The high precision of our derived stellar parameters for HIP 56948 allows us to infer a reasonable estimate of its age from the theoretical isochrones, even though they are densely packed in this main-sequence region.

region around HIP 56948 can potentially host terrestrial planets. The remarkable chemical similarities between HIP 56948 and the Sun, also suggest that HIP 56948 may be capable of hosting rocky planets.

Also, metal-rich solar analogs without close-in giant planets seem to have an abundance pattern closer to solar than stars with detected giant planets (Meléndez et al. 2009)[14].

Our findings open the truly fascinating possibility of identifying Earth-mass planets around other stars based on a careful high resolution spectroscopic analysis of stellar chemical compositions. Once the Kepler mission (e.g. Borucki et al. 2010) announces the discovery of Earth-sized planets in the habitable zones of G-type dwarfs, our planet signature could be verified by high precision chemical abundance analyses of those stars. Although they are relatively faint (confirmed Kepler planet-hosting stars have a mean magnitude of $K_p = 13.8 \pm 1.5$), recently Önehag et al. (2011) have shown that it is possible to achieve high precision (0.03 dex) differential abundances even in stars with $V \approx 15$. They analyzed the faint ($V = 14.6$) solar twin M 67-1194 using VLT/FLAMES-UVES, showing that it has a remarkable chemical similarity to the Sun.

### 4.3. The mass, age, luminosity and radius of HIP 56948

Contrary to common thought, reasonable estimates of the ages of main-sequence stars can be obtained using standard isochrone fitting techniques[15], provided the isochrones are accurate (i.e., calibrated to reproduce the solar age and mass) and the stellar parameters $T_{eff}$, log $g$, [Fe/H] are known with extreme precision, as illustrated in Fig. 9.

We used a fine grid of Yonsei-Yale isochrones (Yi et al. 2001; Kim et al. 2002; Demarque et al. 2004) with a step $\Delta$[Fe/H] = 0.01 dex around solar metallicity ($-0.15 \leq$ [Fe/H] $\leq +0.15$) and a step of $\Delta$[Fe/H] = 0.02 dex elsewhere. We adopt [$\alpha$/Fe] = 0

---

[13] Notice that although this indicates that a certain amount of both Earth-like and meteoritic-like material may have been removed from the Sun (in comparison with the solar twins), this does not imply necessarily that the removed material was employed to form the terrestrial planets and asteroids.

[14] Notice that, as discussed in Schuler et al. (2011) and Ramírez et al. (2010), the interpretation of abundance trends for metal-rich stars is complicated by Galactic chemical evolution processes.

[15] See Baumann et al. (2010); Meléndez et al. (2010c); Bensby et al. (2011); Ramírez et al. (2011); Chanamé & Ramírez (2012), for different applications of our isochrone ages.

for [Fe/H] ≥ 0, [α/Fe] = −0.3 × [Fe/H] for −1 < [Fe/H] < 0, and [α/Fe] = +0.3 for [Fe/H] ≤ −1. The isochrones include a dependence between helium abundance $Y$ and metallicity $Z$ with a slope of 2, $Y = 0.23 + 2Z$ (Yi et al. 2001).

Our grid has been normalized to reproduce the solar age and mass from the input solar parameters ($T_{eff}$ = 5777 K, $\log g$ = 4.44, [Fe/H] = 0.0). The normalization factor was found by performing small offsets around the solar $T_{eff}$, $\log g$ and [Fe/H] to see which offsets better reproduce the solar age and mass. We found that shifts in $T_{eff}$ and $\log g$ are not needed, as the best compromise solution can be found with only a small shift of −0.04 dex in the observed [Fe/H], meaning that the models are off by +0.04 dex in metallicity. Thus, the input metallicity used to compare with the isochrones is:

$$[Fe/H]^{input} = [Fe/H] − 0.04 \text{ dex}. \tag{5}$$

That normalization gives a mean solar mass of 1.000 $M_\odot$ (to within 0.003 $M_\odot$) and a mean solar age of ~4.5 Gyr (to within 0.2 Gyr), which is in excellent agreement with the age of the solar system (~4.567 Gyr, Connelly et al. 2008; Amelin et al. 2010). The calibration of the models to the solar mass and age is valid for a broad range of errors of 10–140 K in $T_{eff}$ and 0.01−0.10 dex both in $\log g$ and [Fe/H]. Thus, after the zero-point shift of Eq. (5) is applied, our resulting masses and ages are accurate. If the input errors are much higher than those indicated above, the zero point of the solutions need to be revised[16].

The isochrone points are characterized by effective temperature ($T$), logarithm of surface gravity ($G$), and metallicity ($M$), with a step in metallicity of 0.01 dex around [Fe/H] = 0.

We obtained an estimate of the age of HIP 56948 from its isochrone age probability distribution (APD):

$$dP(age) = \frac{1}{\Delta(age)} \sum_{\Delta(age)} p\left(T_{eff}, \log g, [Fe/H], T, G, M\right), \tag{6}$$

where $T_{eff}$, $\log g$, [Fe/H] are the observed stellar parameters, $\Delta(age)$ is an adopted step in age from the grid of isochrones, and:

$$p \propto \exp[−(T_{eff} − T)^2/2(\Delta T_{eff})^2]$$
$$\times \exp[−(\log g − G)^2/2(\Delta \log g)^2] \tag{7}$$
$$\times \exp[−([Fe/H] − M)^2/2(\Delta[Fe/H])^2].$$

The errors in observed stellar parameters are $\Delta T_{eff}$, etc. The sum in Eq. (6) is made over a range of isochrone ages and in principle all values of $T, G, M$. In practice, however, the contribution to the sum from isochrone points farther away than $T_{eff} \pm 3\Delta T_{eff}$, etc., is negligible. Therefore, the sum is limited to isochrone points within a radius of three times the errors around the observed stellar parameters. A similar formalism allows us to infer the stellar mass. The probability distributions are normalized so that $\sum dP = 1$. The most probable age and mass are obtained from the peaks of these distributions while $1\sigma$ and $2\sigma$ Gaussian-like lower and upper limits can be derived from the shape of the probability distributions.

---

[16] For errors of 175 K in $T_{eff}$ and 0.1 dex both in $\log g$ and [Fe/H], the solar mass and age would be about 0.99 $M_\odot$ and 4.8 Gyr, while for an error of 250 K in $T_{eff}$ and 0.15 dex both in $\log g$ and [Fe/H], the solar mass and age would be about 0.98 $M_\odot$ and 5.5 Gyr, respectively. However, for typical errors of abundance analysis of $\sigma(T_{eff})$ < 150 K, $\sigma(\log g)$ ≤ 0.1 dex and $\sigma([Fe/H])$ ≤ 0.1 dex, no zero-point corrections (besides that already used in Eq. (5)) would be needed to obtain accurate masses and ages.
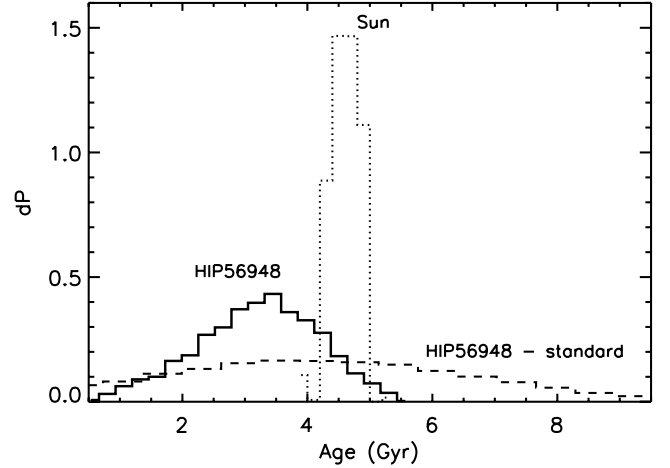


**Fig. 10.** Age probability distributions (APDs) for the Sun (dotted line) and HIP 56948 (solid line). The dashed line corresponds to the APD that we would obtain for HIP 56948 if we had derived its stellar parameters from photometric data and Hipparcos parallax (the "standard" method) instead of performing our very precise strict differential analysis. Clearly, our differential approach gives much better results.

Figure 10 shows the APDs of the Sun and HIP 56948. For HIP 56948 we adopted errors from our differential analysis relative to the Sun of 7 K in $T_{eff}$, 0.02 dex in $\log g$, and 0.01 dex in [Fe/H], while for the Sun we adopted errors of 5 K in $T_{eff}$ and 0.005 dex in $\log g$ and [Fe/H]. Although the errors for the Sun are overestimated, they allow us to obtain a smooth APD.

Using our precisely determined stellar parameters for HIP 56948, we derive a most probable age of 3.45 Gyr. The $1\sigma$ range of ages is 2.26–4.12 Gyr whereas the $2\sigma$ range of ages is 1.25–4.92 Gyr. Notice that although the adopted He abundance may have some influence on the derived age, our small error bars in the stellar parameters of HIP 56948, rule out radically different He abundances. For relatively small changes in He, the effect on the derived stellar age is relatively minor. This is discussed in detail in Appendix D, where stellar tracks with different He abundances are presented. The mass is much better constrained; for HIP 56948 we derive 1.020 ± 0.016 $M_\odot$ ($2\sigma$ error).

In Fig. 10 we also show the APD of HIP 56948 assuming that its parameters were obtained using standard methods, for example obtaining $T_{eff}$ from photometric data and $\log g$ from the Hipparcos parallax. The standard methods imply an error of at least 100 K in $T_{eff}$ due to uncertainties in the zero-point of color-$T_{eff}$ relations (Casagrande et al. 2010; Meléndez et al. 2010b), while the error in Hipparcos parallax and typical errors in mass, $T_{eff}$ and $V$ magnitude imply a total error of about 0.07 dex in $\log g$. For the error in [Fe/H] of a typical abundance analysis we adopt 0.05 dex. Clearly, in this case the age of HIP 56948 is not well constrained. At most, we can say that the star is likely younger than about 8 Gyr. Thus, another advantage of studying solar twins using very high quality spectroscopic data and strict differential analysis is that useful estimates of their ages can be obtained with the classical isochrone method, which can be a valuable asset for a variety of studies (e.g., Baumann et al. Baumann et al. (2010)).

The luminosity of HIP 56948 can be estimated from:

$$\log L/L_\odot = \log(M/M_\odot) − (\log g − 4.44) + 4 \log(T_{eff}/5777) \tag{8}$$

where $M$ is the stellar mass and $L$ the luminosity. Using our precise stellar parameters and mass we find $L = 0.986 \pm 0.051\ L_\odot$.

Thus, the luminosity of HIP 56948 is essentially solar and therefore the extent of its habitable zone should be similar to the habitable region around the Sun (Kasting et al. 1993). From $L = 4\pi R^2 \sigma T_{eff}^4$, we find a radius of $R = 0.987 \pm 0.023\,R_\odot$, i.e., solar within the error bars.

### 4.4. Further constraints on the age of HIP 56948

Additional insight on the age of HIP 56948 can be obtained from its chromospheric activity (Soderblom 2010), lithium abundance (do Nascimento et al. 2009; Baumann et al. 2010) and gyrochronology (Barnes 2007).

Determination of stellar ages based on chromospheric activity may only be valid for solar type stars younger than ~2 Gyr (Pace & Pasquini 2004; Pace et al. 2009; Zhao et al. 2011), as older stars show a low activity level which changes little with increasing age. Chromospheric activity is thus mainly useful to distinguish young and old stars. A measurement of chromospheric activity for HIP 56948 was obtained by Meléndez & Ramírez (2007) based on observations taken in April 2007, resulting in a low chromospheric $S$-value of $S = 0.165\ (\pm 0.013)$ in the Mount Wilson scale. Using another observation taken in November 2007 we find a similar value, $S = 0.170\ (\pm 0.013)$. Both values are as low as the the mean chromospheric activity index in the Sun, $\langle S_\odot \rangle = 0.179$ (Baliunas et al. 1995). The low $S$-value of HIP 56948 suggests that it should be older than ~2 Gyr.

Although it is well-known that lithium steeply decays with age in very young stars (Soderblom 2010), only recently it has been observationally shown that the decay continues for older ages (Meléndez et al. 2010a; Baumann et al. 2010), as already predicted by several models of non-standard Li depletion (Montalbán & Schatzman 2000; Charbonnel & Talon 2005; do Nascimento et al. 2009; Xiong & Deng 2009; Denissenkov 2010). Unfortunately, we cannot determine stellar ages with the required precision to discern to what extent there is a spread (or not) in the age-lithium relation, although the most precise values available (Ramírez et al. 2011; this work; Meléndez et al. 2012, in prep.) show relatively little dispersion (Fig. 11). Theoretical Li-age relations can be used to check if a lithium age is compatible with the age determined from isochrones. In Fig. 11 we compare several Li theoretical tracks (Charbonnel & Talon 2005; do Nascimento et al. 2009; Xiong & Deng 2009; Denissenkov 2010) with our NLTE Li abundances and isochrone ages. As can be seen, the agreement is excellent. If we were to derive an age for HIP 56948 based on the theoretical Li-age relations, it would be $3.62 \pm 0.19$ Gyr, i.e., almost the same age determined using isochrones. This comparison give us further confidence that HIP 56948 is about 1 Gyr younger than the Sun. Although the scatter of the Li age obtained using different Li tracks is relatively small (0.19 Gyr), we conservatively assign an error of 1.0 Gyr to the Li-age, to take into account any possible observational spread of the Li-age relation around solar age (Fig. 11).

Stellar rotation can be used to estimate a rotational age (Barnes 2007; Soderblom 2010). Unfortunately there is no information on the rotation period of HIP 56948 yet. Nevertheless, $v \sin i$ can give us an upper limit on the rotation period, thus allowing us to infer an upper limit on the age. The determination of $v \sin i$ is based on the differential line broadening between HIP 56948 and the Sun, as described in Appendix E.

We infer for HIP 56948 $v \sin i / v \sin i_\odot = 1.006 \pm 0.014$, or $\Delta v \sin i = +0.013 \pm 0.026$ km s$^{-1}$ (or $\pm 0.032$ km s$^{-1}$ including the error in macroturbulence), i.e., HIP 56948 seems to have
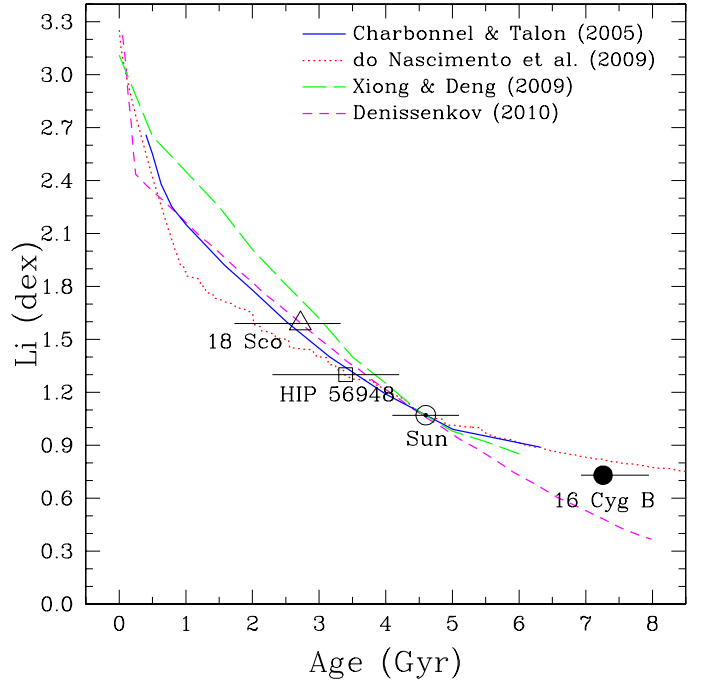


**Fig. 11.** Li vs. age for the Sun ($\odot$) and HIP 56948 (square) based on our NLTE Li abundances and isochrone ages, and for 16 Cyg B (filled circle) and 18 Sco (triangle, 2.7 Gyr$_{+0.6}^{-1.0}$), based on similar quantities by Ramírez et al. (2011) and Meléndez et al. (2012, in prep.). The total error bar ($\pm \sigma$) of the Li abundance is about the size of the symbols, while the error bars in age are shown by horizontal lines. For comparison we show the models by Charbonnel & Talon (2005); do Nascimento et al. (2009); Xiong & Deng (2009); Denissenkov (2010), shifted in Li abundance by 0.00, $-0.03$, $-0.15$, $-0.05$ dex, respectively, to reproduce our observed NLTE solar Li abundance. The age of HIP 56948 based on Li tracks is in perfect agreement with the age obtained from isochrones.

about the same rotation velocity as the Sun. Within the uncertainties we infer that HIP 56948 cannot be older than the Sun. Using the relation between rotation period and age given in Meléndez et al. (2006) and Barnes (2007), we find an upper limit of age $\leq 4.7$ Gyr.

Figure 12 summarizes our findings on the age of HIP 56948. Our precise stellar parameters and differential isochrone analysis result in an age of $3.45 \pm 0.93$ Gyr (1-$\sigma$ error). The somewhat higher Li abundance of HIP 56948 with respect to the Sun indicates an age of ~$3.62 \pm 1.00$ Gyr. Chromospheric activity gives a lower limit of 2 Gyr, while $v \sin i$ suggests an upper limit of 4.7 Gyr. In Fig. 12 we show the combined age probability distribution. Based on all the above indicators we suggest an age of $3.52 \pm 0.68$ Gyr for HIP 56948.

Age is a key parameter for SETI programs (Turnbull & Tarter 2003), as stars only 1–2 Gyr old may not have had enough time to develop complex life. Life on Earth apparently appeared within the first billion year of the Earth's formation (Schopf 1993; Mojzsis et al. 1996; McKeegan et al. 2007; Abramov & Mojzsis 2009), but there is no consensus on the exact date. Undisputed evidence for life can be traced back to about 2.7 Gyrs ago (e.g., see review by López-Garcia et al. 2006). Yet, complex life only appeared about 0.5–1 Gyr ago (Wray et al. 1996; Seilacher et al. 1998; Rasmussen et al. 2002; Marshall 2006). HIP 56948 is about one billion years younger than the Sun, so assuming a similar evolution path as that of life on Earth, complex life may be just developing (or already sprung
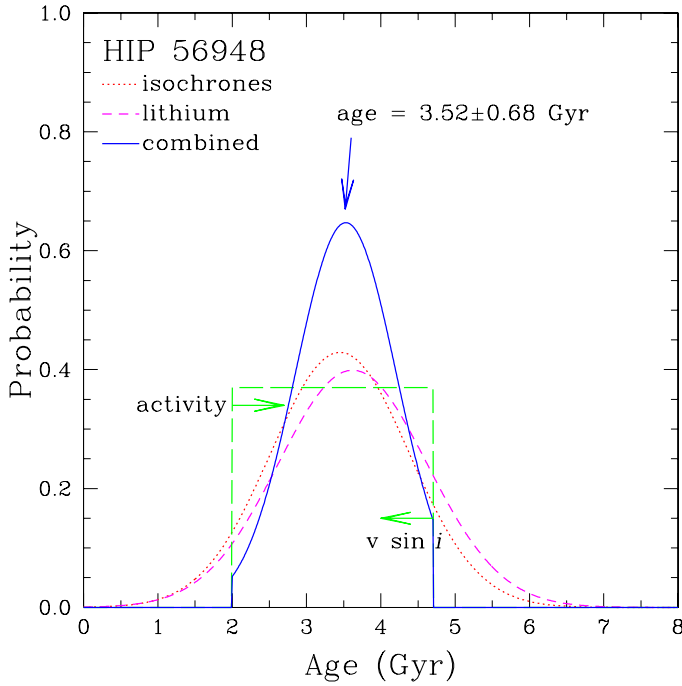
**Fig. 12.** Age probability distributions for HIP 56948 based on isochrones (dotted line) and lithium abundance (dashed line). The limits on age imposed by chromospheric activity and by rotation ($v \sin i$) are also shown (long dashed lines). The combined age probability distribution (solid line) is centered at 3.52 Gyr and has $\sigma = 0.68$ Gyr.

if complexity elsewhere can arise earlier than on Earth) on any hypothetical Earth that this star may host.

## 5. Conclusions

We have shown that using spectra of superb quality coupled to a fully differential analysis of solar twins and the Sun, it is possible to achieve measurements errors as low as 0.003 dex for several elements (Si, Ca, Ti, Cr, Fe, Co, Ni). Considering also the uncertainties in stellar parameters, we achieve an unprecedented accuracy of only ∼0.005 dex (1%) in relative abundances for some elements and <0.01 dex for most elements. This is almost one order of magnitude better than state-of-the-art works in terms of absolute abundances (e.g., Asplund 2005; Asplund et al. 2009).

The star HIP 56948 is remarkably similar to the Sun in many different aspects. The effective temperature, $\log g$, metallicity and microturbulence are very similar. The similarities also extend to its detailed chemical abundance pattern. The volatile elements are in excellent agreement, but the refractory elements are slightly (0.01 dex) more enhanced relative to the volatile elements in HIP 56948. From the comparison with the abundances of Earth-like and chondrite-like material, we infer that about twice as much rocky material may have formed around the Sun than around HIP 56948, albeit the amount of Earth-like material is comparable for both stars (∼2 $M_\oplus$). The mass, luminosity and radius of HIP 56948 are essentially solar within the uncertainties. Lithium is severely depleted in HIP 56948, but not as much as in the Sun, as expected for a solar twin somewhat younger than the Sun. Finally, our precise radial velocity data shows that the inner region around HIP 56948 is free from giant planets, making thus more likely the existence of terrestrial planets around this remarkable solar twin. Considering its similarities to our Sun and its mature age, we urge the community

to closely monitor HIP 56948 for planet and SETI searches, and to use other techniques that could further our knowledge about HIP 56948, such as for example asteroseismology, that have provided important constraints for the solar twin 18 Sco (Bazot et al. 2011).

The abundances anomalies we have discussed here cannot be explained by contamination from AGB stars, SNIa, SNII or HN (Sect. 4), or by Galactic chemical evolution processes or age effects (Meléndez et al. 2009). Kiselman et al. (2011) have shown that the peculiar abundance pattern cannot be attributed to line-of-sight inclination effects. Also, the abundance trend does not arise due to the particular reflection properties of asteroids (appendix B). Although the abundance peculiarities may indicate that the Sun was born in a massive open cluster like M 67 (Önehag et al. 2011), this explanation is based on the analysis of only one solar twin. The Uppsala group is leading a high precision abundance study of other solar twins in M 67, in order to confirm or reject this hypothesis. So far the best explanation for the abundance trend seems to be the formation of terrestrial planets. The Kepler mission should detect the first Earth-sized planets in the habitable zones of solar type stars. We look forward to using 8−10 m telescopes to perform careful differential abundance analyses of those stars, in order to verify if our chemical signatures indeed imply rocky planets.

## References

Abramov, O., & Mojzsis, S. J. 2009, Nature, 459, 419
Adams, F. C. 2010, ARA&A, 48, 47
Allende Prieto, C., Lambert, D. L., & Asplund, M. 2001, ApJ, 556, L63
Allende Prieto, C., Barklem, P. S., Lambert, D. L., & Cunha, K. 2004, A&A, 420, 183
Amelin, Y., Kaltenbach, A., Iizuka, T., et al. 2010, Earth Planet. Sci. Lett., 300, 343
Anders, E., & Grevesse, N. 1989, Geochim. Cosmochim. Acta, 53, 197
Andersen, J., Gustafsson, B., & Lambert, D. L. 1984, A&A, 136, 65
Asplund, M. 2005, ARA&A, 43, 481
Asplund, M., Grevesse, N., Sauval, A. J., Allende Prieto, C., & Kiselman, D. 2004, A&A, 417, 751
Asplund, M., Grevesse, N., Sauval, A. J., & Scott, P. 2009, ARA&A, 47, 481
Baliunas, S. L., Donahue, R. A., Soon, W. H., et al. 1995, ApJ, 438, 269
Baraffe, I., & Chabrier, G. 2010, A&A, 521, A44
Barklem, P. S., & Aspelund-Johansson, J. 2005, A&A, 435, 373
Barklem, P. S., Piskunov, N., & O'Mara, B. J. 2000, A&AS, 142, 467
Barnes, S. A. 2007, ApJ, 669, 1167
Baumann, P., Ramírez, I., Meléndez, J., Asplund, M., & Lind, K. 2010, A&A, 519, A87
Bautista, M. A. 1997, A&AS, 122, 167
Bazot, M., Ireland, M. J., Huber, D., et al. 2011, A&A, 526, L4

Bensby, T., Adén, D., Meléndez, J., et al. 2011, A&A, 533, A134
Bergemann, M. 2011, MNRAS, 413, 2184
Bergemann, M., & Cescutti, G. 2010, A&A, 522, A9
Bergemann, M., & Gehren, T. 2008, A&A, 492, 823
Bergemann, M., Pickering, J. C., & Gehren, T. 2010, MNRAS, 401, 1334
Bergemann, M., et al. 2012, submitted
Bessell, M. S., Castelli, F., & Plez, B. 1998, A&A, 333, 231
Binzel, R. P., Bus, S. J., Burbine, T. H., & Sunshine, J. M. 1996, Science, 273, 946
Borucki, W. J., Koch, D., Basri, G., et al. 2010, Science, 327, 977
Boss, A. P., & Foster, P. N. 1998, ApJ, 494, L103
Bus, S. J., & Binzel, R. P. 2002, Icarus, 158, 146
Busso, M., Gallino, R., & Wasserburg, G. J. 1999, ARA&A, 37, 239
Cameron, A. G. W., & Truran, J. W. 1977, Icarus, 30, 447
Carlsson, M. 1986, Uppsala Astronomical Observatory Reports, 33
Casagrande, L., Ramírez, I., Meléndez, J., Bessell, M., & Asplund, M. 2010, A&A, 512, A54
Casagrande, L., Schönrich, R., Asplund, M., et al. 2011, A&A, 530, A138
Castelli, F., Gratton, R. G., & Kurucz, R. L. 1997, A&A, 318, 841
Castro, M., Vauclair, S., & Richard, O. 2007, A&A, 463, 755
Castro, M., Do Nascimento, J. D., Jr., Biazzo, K., Meléndez, J., & de Medeiros, J. R. 2011, A&A, 526, A17
Cayrel de Strobel, G. 1996, A&ARv, 7, 243
Chaboyer, B., Fenton, W. H., Nelan, J. E., Patnaude, D. J., & Simon, F. E. 2001, ApJ, 562, 521
Chambers, J. E. 2010, ApJ, 724, 92
Chambers, J. E., & Wetherill, G. W. 2001, Meteor. Planet. Sci., 36, 381
Chanamé, J., & Ramírez, I. 2012, ApJ, 746, 102
Charbonnel, C., & Talon, S. 2005, Science, 309, 2189
Connelly, J. N., Amelin, Y., Krot, A. N., & Bizzarro, M. 2008, ApJ, 675, L121
Cox, A. N. 2000, Allen's Astrophysical Quantities, 4th edn (New York: AIP Press/Springer)
Demarque, P., Woo, J.-H., Kim, Y.-C., & Yi, S. K. 2004, ApJS, 155, 667
DeMeo, F. E., Binzel, R. P., Slivan, S. M., & Bus, S. J. 2009, Icarus, 202, 160
Denissenkov, P. A. 2010, ApJ, 719, 28
Do Nascimento, J. D., Jr., Castro, M., Meléndez, J., et al. 2009, A&A, 501, 687
Drawin, H.-W. 1968, Z. Phys., 211, 404
Drawin, H. W. 1969, Z. Phys., 225, 483
Dumusque, X., Udry, S., Lovis, C., Santos, N. C., & Monteiro, M. J. P. F. G. 2011, A&A, 525, A140
Endl, M., Kürster, M., & Els, S. 2000, A&A, 362, 585
Endl, M., Cochran, W. D., Wittenmyer, R. A., & Hatzes, A. P. 2006, AJ, 131, 3131
Fabbian, D., Asplund, M., Carlsson, M., & Kiselman, D. 2006, A&A, 458, 899
Fabbian, D., Asplund, M., Barklem, P. S., Carlsson, M., & Kiselman, D. 2009, A&A, 500, 1221
Fuhr, J. R., & Wiese, W. L. 2006, J. Phys. Chem. Ref. Data, 35, 1669
Gehren, T., Liang, Y. C., Shi, J. R., Zhang, H. W., & Zhao, G. 2004, A&A, 413, 1045
Gehren, T., Shi, J. R., Zhang, H. W., Zhao, G., & Korn, A. J. 2006, A&A, 451, 1065
Giddings, J. R. 1981, Ph.D. Thesis
Gonzalez, G., Carlson, M. K., & Tobin, R. W. 2010, MNRAS, 407, 314
González Hernández, J. I., Israelian, G., Santos, N. C., et al. 2010, ApJ, 720, 1592
Gray, D. F. 2005, The Observation and Analysis of Stellar Photospheres, 3rd edn. (Cambridge, UK: Cambridge University Press)
Gray, D. F., Tycner, C., & Brown, K. 2000, PASP, 112, 328
Grupp, F. 2004, A&A, 420, 289
Guenther, D. B., Demarque, P., Kim, Y.-C., & Pinsonneault, M. H. 1992, ApJ, 387, 372
Gustafsson, B. 2008, Phys. Scr. T, 130, 014036
Gustafsson, B., Edvardsson, B., Eriksson, K., et al. 2008, A&A, 486, 951
Gustafsson, B., Meléndez, J., Asplund, M., & Yong, D. 2010, Ap&SS, 328, 185
Guzik, J. A., & Mussack, K. 2010, ApJ, 713, 1108
Hekker, S., & Meléndez, J. 2007, A&A, 475, 1003
Hobbs, L. M., Thorburn, J. A., & Rebull, L. M. 1999, ApJ, 523, 797
Karakas, A. I. 2010, MNRAS, 403, 1413
Karakas, A., & Lattanzio, J. C. 2007, PASA, 24, 103
Kasting, J. F., Whitmire, D. P., & Reynolds, R. T. 1993, Icarus, 101, 108
Kim, Y.-C., Demarque, P., Yi, S. K., & Alexander, D. R. 2002, ApJS, 143, 499
Kiselman, D., Pereira, T. M. D., Gustafsson, B., et al. 2011, A&A, 535, A14
Kobayashi, C., & Nakasato, N. 2011, ApJ, 729, 16
Kobayashi, C., & Nomoto, K. 2009, ApJ, 707, 1466
Kobayashi, C., Umeda, H., Nomoto, K., Tominaga, N., & Ohkubo, T. 2006, ApJ, 653, 1145

Kupka, F. G., Ryabchikova, T. A., Piskunov, N. E., Stempels, H. C., & Weiss, W. W. 2000, Baltic Astron., 9, 590
Lazzaro, D., Angeli, C. A., Carvano, J. M., et al. 2004, Icarus, 172, 179
Li, T. D., Bi, S. L., Chen, Y. Q., et al. 2012, ApJ, 746, 143
Lind, K., Asplund, M., & Barklem, P. S. 2009, A&A, 503, 541
Lind, K., Asplund, M., Barklem, P. S., & Belyaev, A. K. 2011a, A&A, 528, A103
Lind, K., Charbonnel, C., Decressin, T., et al. 2011b, A&A, 527, A148
Lodders, K. 2003, ApJ, 591, 1220
López-Garcia, P., Moreira, D., Douzery, E., et al. 2006, Earth Moon Planets, 98, 247
Mandell, A. M., Ge, J., & Murray, N. 2004, AJ, 127, 1147
Marshall, C. R. 2006, Ann. Rev. Earth Planet. Sci., 34, 355
Masana, E., Jordi, C., & Ribas, I. 2006, A&A, 450, 735
Mashonkina, L., Korn, A. J., & Przybilla, N. 2007, A&A, 461, 261
Mashonkina, L., Gehren, T., Shi, J., Korn, A., & Grupp, F. 2010, IAU Symp., 265, 197
Mashonkina, L., Gehren, T., Shi, J.-R., Korn, A. J., & Grupp, F. 2011, A&A, 528, A87
McKeegan, K. D., Kudryavtsev, A. B. & Schopf, J. W. 2007, Geology, 35, 591
Meléndez, J., & Asplund, M. 2008, A&A, 490, 817
Meléndez, J., & Barbuy, B. 1999, ApJS, 124, 527
Meléndez, J., & Barbuy, B. 2009, A&A, 497, 611
Meléndez, J., & Cohen, J. G. 2007, ApJ, 659, L25
Meléndez, J., & Cohen, J. G. 2009, ApJ, 699, 2017
Meléndez, J., & Ramírez, I. 2007, ApJ, 669, L89
Meléndez, J., Dodds-Eden, K., & Robles, J. A. 2006, ApJ, 641, L133
Meléndez, J., Asplund, M., Gustafsson, B., & Yong, D. 2009, ApJ, 704, L66
Meléndez, J., Ramírez, I., Casagrande, L., et al. 2010a, Ap&SS, 328, 193
Meléndez, J., Schuster, W. J., Silva, J. S., et al. 2010b, A&A, 522, A98
Meléndez, J., Casagrande, L., Ramírez, I., Asplund, M., & Schuster, W. J. 2010c, A&A, 515, L3
Metcalfe, T. S., Chaplin, W. J., Appourchaux, T., et al. 2012, ApJ, 748, L10
Miki, J., Takigawa, A., Tachibana, S., & Huss, G. R. 2007, Lun. Planet. Inst. Sci. Conf. Abstracts, 38, 1493
Minton, D. A., & Malhotra, R. 2010, Icarus, 207, 744
Mojzsis, S. J., Arrhenius, G., McKeegan, K. D., et al. 1996, Nature, 384, 55
Montalbán, J., & Schatzman, E. 2000, A&A, 354, 943
Neves, V., Santos, N. C., Sousa, S. G., Correia, A. C. M., & Israelian, G. 2009, A&A, 497, 563
Nissen, P. E., & Schuster, W. J. 2010, A&A, 511, L10
Nordlund, A. 2009 [arXiv:0908.3479]
Olsen, E. H. 1993, A&AS, 102, 89
Önehag, A., Korn, A., Gustafsson, B., Stempels, E., & Vandenberg, D. A. 2011, A&A, 528, A85
Ouellette, N., Desch, S. J., & Hester, J. J. 2010, ApJ, 711, 597
Pace, G., & Pasquini, L. 2004, A&A, 426, 1021
Pace, G., Melendez, J., Pasquini, L., et al. 2009, A&A, 499, L9
Pasquini, L., Biazzo, K., Bonifacio, P., Randich, S., & Bedin, L. R. 2008, A&A, 489, 677
Pereira, T. M. D., Asplund, M., & Kiselman, D. 2009, A&A, 508, 1403
Petit, J.-M., Morbidelli, A., & Valsecchi, G. B. 1999, Icarus, 141, 367
Pichardo, B., Moreno, E., Allen, C., et al. 2012, AJ, 143, 73
Porto de Mello, G. F., & da Silva, L. 1997, ApJ, 482, L89
Ramírez, I., Meléndez, J., & Asplund, M. 2009, A&A, 508, L17
Ramírez, I., Asplund, M., Baumann, P., Meléndez, J., & Bensby, T. 2010, A&A, 521, A33
Ramírez, I., Meléndez, J., Cornejo, D., Roederer, I. U., & Fish, J. R. 2011, ApJ, 740, 76
Ramirez, I., Michel, R., Sefako, R., et al. 2012, ApJ, 752, 5
Rasmussen, B., Bengtson, S., Fletcher, I. R., & McNaughton, N. J. 2002, Science, 296, 1112
Reddy, B. E., Tomkin, J., Lambert, D. L., & Allende Prieto, C. 2003, MNRAS, 340, 304
Robertson, P., Endl, M., Cochran, W. D., et al. 2012, ApJ, 749, 39
Saar, S. H., & Osten, R. A. 1997, MNRAS, 284, 803
Schopf, J. W. 1993, Science, 260, 640
Schuler, S. C., Flateau, D., Cunha, K., et al. 2011, ApJ, 732, 55
Seilacher, A., Bose, P. K., & Pflueger, F. 1998, Science, 282, 80
Serenelli, A. M., Haxton, W. C., & Peña-Garay, C. 2011, ApJ, 743, 24
Smith, V. V., Lambert, D. L., & Nissen, P. E. 1998, ApJ, 506, 405
Sneden, C. A. 1973, Ph.D. Thesis,
Soderblom, D. R. 2010, ARA&A, 48, 581
Soubiran, C., & Triaud, A. 2004, A&A, 418, 1089
Sousa, S. G., Santos, N. C., Israelian, G., Mayor, M., & Monteiro, M. J. P. F. G. 2007, A&A, 469, 783
Stromgren, B., Gustafsson, B., & Olsen, E. H. 1982, PASP, 94, 5

Takeda, Y. 2007, PASJ, 59, 335

Takeda, Y., & Tajitsu, A. 2009, PASJ, 61, 471

Takeda, Y., Zhao, G., Chen, Y.-Q., Qiu, H.-M., & Takada-Hidai, M. 2002, PASJ, 54, 275

Takeda, Y., Hashimoto, O., Taguchi, H., et al. 2005, PASJ, 57, 751

Takeda, Y., Kawanomoto, S., Honda, S., Ando, H., & Sakurai, T. 2007, A&A, 468, 663

Tull, R. G., MacQueen, P. J., Sneden, C., & Lambert, D. L. 1995, PASP, 107, 251

Turnbull, M. C., & Tarter, J. C. 2003, ApJS, 145, 181

Trigo-Rodríguez, J. M., García-Hernández, D. A., Lugaro, M., et al. 2009, Meteorit. Planet. Sci., 44, 627

Valenti, J. A., & Fischer, D. A. 2005, ApJS, 159, 141

van Leeuwen, F. 2007, A&A, 474, 653

Velichko, A. B., Mashonkina, L. I., & Nilsson, H. 2010, Astron. Lett., 36, 664

Vogt, S. S., Allen, S. L., Bigelow, B. C., et al. 1994, Proc. SPIE, 2198, 362

Wasserburg, G. J., Busso, M., Gallino, R., & Raiteri, C. M. 1994, ApJ, 424, 412

Weidenschilling, S. J. 1977, Ap&SS, 51, 153

Wetherill, G. W. 1989, In Asteroids II, ed. R. P. Binzel, T. Gehrels, & M. S. Matthews (Tucson: Univ. of Arizona Press), 661

Wetherill, G. W. 1992, Icarus, 100, 307

Wray, G. A., Levinton, J. S., & Shapiro, L. H. 1996, Science, 274, 568

Wright, J. T. 2005, PASP, 117, 657

Xiong, D. R., & Deng, L. 2009, MNRAS, 395, 2013

Xu, S., Binzel, R. P., Burbine, T. H., & Bus, S. J. 1995, Icarus, 115, 1

Yi, S., Demarque, P., Kim, Y.-C., et al. 2001, ApJS, 136, 417

Yong, D., Grundahl, F., Lambert, D. L., Nissen, P. E., & Shetrone, M. D. 2003, A&A, 402, 985

Yong, D., Grundahl, F., Nissen, P. E., Jensen, H. R., & Lambert, D. L. 2005, A&A, 438, 875

Young, E. D., Gounelle, M., Smith, R. L., Morris, M. R., & Pontoppidan, K. M. 2011, ApJ, 729, 43

Zhao, J. K., Oswalt, T. D., Rudkin, M., Zhao, G., & Chen, Y. Q. 2011, AJ, 141, 107

**Table 1.** McDonald radial velocity measurements for HIP 56948.

| BJD (m s$^{-1}$) | Velocity (m s$^{-1}$) | Error |
|---|---|---|
| 2 454 250.742247 | 1.86 | 3.51 |
| 2 454 251.762237 | 6.18 | 6.37 |
| 2 454 347.603043 | –0.26 | 8.35 |
| 2 454 822.022016 | –3.17 | 4.48 |
| 2 455 285.780573 | 6.53 | 6.00 |
| 2 455 585.972936 | –5.06 | 4.07 |
| 2 455 643.770312 | –0.17 | 4.67 |
| 2 455 667.816687 | –16.11 | 4.17 |
| 2 455 990.845569 | 10.21 | 5.51 |

**Table 2.** Keck radial velocity measurements for HIP 56948.

| BJD (m s$^{-1}$) | Velocity (m s$^{-1}$) | Error |
|---|---|---|
| 2 455 610.068981 | –2.77 | 3.24 |
| 2 455 611.013099 | –6.06 | 3.73 |
| 2 455 611.100610 | –9.49 | 3.38 |
| 2 455 611.148864 | –10.18 | 3.83 |
| 2 455 766.748023 | 5.54 | 2.20 |
| 2 455 767.742970 | 4.39 | 2.65 |
| 2 455 767.746153 | 0.82 | 3.78 |
| 2 455 767.749454 | 3.74 | 2.00 |
| 2 455 935.157734 | –0.35 | 2.43 |
| 2 455 935.160951 | 1.21 | 1.89 |
| 2 455 935.163959 | 0.67 | 2.34 |
| 2 455 936.135676 | –4.52 | 3.28 |
| 2 455 936.138532 | –5.07 | 1.98 |
| 2 455 936.141412 | –8.27 | 2.68 |
| 2 455 937.130793 | 0.19 | 2.85 |
| 2 455 937.133891 | –1.58 | 2.46 |
| 2 455 937.137006 | –1.07 | 2.54 |
| 2 455 938.111144 | 3.23 | 3.62 |
| 2 455 938.114027 | 3.34 | 2.50 |
| 2 455 938.116890 | –2.13 | 4.05 |
| 2 455 962.089413 | 1.70 | 2.95 |
| 2 455 962.092257 | 0.20 | 2.62 |
| 2 455 962.095094 | 0.85 | 1.84 |
| 2 455 963.104952 | 3.75 | 3.12 |
| 2 455 963.107611 | 5.20 | 1.86 |
| 2 455 963.110271 | 1.18 | 2.34 |
| 2 455 964.037962 | 1.92 | 2.66 |
| 2 455 965.071634 | 3.50 | 1.98 |
| 2 455 965.075176 | 4.35 | 3.92 |
| 2 455 965.078440 | 5.71 | 2.31 |

**Table 3.** Adopted atomic data, equivalent widths, and differential NLTE corrections (HIP 56948 – Sun).

| Wavelength (Å) | ion | $\chi_{exc}$ (eV) | $\log gf$ | $C_6$ | EW HIP 56948 | EW Sun | ΔNLTE (dex) |
|---|---|---|---|---|---|---|---|
| 4445.471 | 26.00 | 0.087 | –5.441 | 2.80 | 40.1 | 40.8 | 0.001 |
| 5044.211 | 26.00 | 2.8512 | –2.058 | 0.271E-30 | 73.7 | 73.6 | 0.001 |
| 5225.525 | 26.00 | 0.1101 | –4.789 | 0.123E-31 | 71.2 | 70.4 | 0.000 |
| 5247.050 | 26.00 | 0.0872 | –4.946 | 0.122E-31 | 66.0 | 66.3 | 0.001 |
| 5250.208 | 26.00 | 0.1212 | –4.938 | 0.123E-31 | 64.7 | 64.9 | 0.001 |
| 5651.469 | 26.00 | 4.473 | –1.75 | 0.483E-30 | 19.3 | 18.9 | 0.001 |
| 5661.348 | 26.00 | 4.2843 | –1.756 | 0.324E-30 | 23.7 | 22.8 | 0.001 |
| 5679.023 | 26.00 | 4.652 | –0.75 | 0.813E-30 | 59.9 | 59.4 | 0.000 |
| 5696.089 | 26.00 | 4.548 | –1.720 | 0.578E-30 | 14.4 | 13.9 | 0.000 |
| 5701.544 | 26.00 | 2.559 | –2.216 | 0.495E-31 | 85.7 | 84.2 | 0.001 |
| 5705.464 | 26.00 | 4.301 | –1.355 | 0.302E-30 | 38.2 | 38.0 | 0.001 |
| 5778.453 | 26.00 | 2.588 | –3.430 | 0.495E-31 | 22.6 | 22.5 | 0.001 |
| 5784.658 | 26.00 | 3.396 | –2.532 | 0.357E-30 | 27.1 | 27.1 | 0.000 |
| 5793.914 | 26.00 | 4.220 | –1.619 | 0.272E-30 | 34.6 | 33.9 | 0.000 |
| 5809.218 | 26.00 | 3.883 | –1.609 | 0.565E-30 | 51.9 | 51.2 | 0.000 |
| 5855.076 | 26.00 | 4.6075 | –1.478 | 0.574E-30 | 23.8 | 23.1 | 0.000 |
| 5916.247 | 26.00 | 2.453 | –2.936 | 0.429E-31 | 56.5 | 55.8 | 0.001 |
| 5956.694 | 26.00 | 0.8589 | –4.605 | 0.155E-31 | 50.8 | 50.9 | 0.001 |
| 6027.050 | 26.00 | 4.0758 | –1.09 | 2.80 | 64.7 | 63.9 | 0.001 |
| 6065.482 | 26.00 | 2.6085 | –1.530 | 0.471E-31 | 117.6 | 117.2 | 0.001 |
| 6093.644 | 26.00 | 4.607 | –1.30 | 0.441E-30 | 32.0 | 31.6 | 0.001 |
| 6096.665 | 26.00 | 3.9841 | –1.81 | 0.575E-30 | 38.1 | 37.1 | 0.000 |
| 6151.618 | 26.00 | 2.1759 | –3.299 | 0.255E-31 | 50.6 | 49.7 | 0.000 |
| 6165.360 | 26.00 | 4.1426 | –1.46 | 2.80 | 46.1 | 44.9 | 0.000 |
| 6173.335 | 26.00 | 2.223 | –2.880 | 0.265E-31 | 69.2 | 68.8 | 0.001 |
| 6200.313 | 26.00 | 2.6085 | –2.437 | 0.458E-31 | 75.1 | 74.3 | 0.000 |
| 6213.430 | 26.00 | 2.2227 | –2.52 | 0.262E-31 | 83.5 | 82.3 | 0.000 |
| 6219.281 | 26.00 | 2.198 | –2.433 | 0.258E-31 | 90.3 | 89.0 | 0.001 |
| 6240.646 | 26.00 | 2.2227 | –3.233 | 0.314E-31 | 49.2 | 49.4 | 0.001 |
| 6252.555 | 26.00 | 2.4040 | –1.687 | 0.384E-31 | 121.3 | 120.7 | 0.001 |
| 6265.134 | 26.00 | 2.1759 | –2.550 | 0.248E-31 | 84.9 | 85.2 | 0.001 |
| 6270.225 | 26.00 | 2.8580 | –2.54 | 0.458E-31 | 51.4 | 51.4 | 0.001 |
| 6430.846 | 26.00 | 2.1759 | –2.006 | 0.242E-31 | 112.6 | 111.2 | 0.001 |
| 6498.939 | 26.00 | 0.9581 | –4.699 | 0.153E-31 | 46.9 | 46.4 | 0.000 |
| 6593.871 | 26.00 | 2.4326 | –2.422 | 0.369E-31 | 83.5 | 83.6 | 0.001 |
| 6703.567 | 26.00 | 2.7585 | –3.023 | 0.366E-31 | 37.6 | 37.5 | 0.001 |
| 6705.102 | 26.00 | 4.607 | –0.98 | 2.80 | 47.3 | 47.6 | 0.001 |
| 6713.745 | 26.00 | 4.795 | –1.40 | 0.430E-30 | 21.8 | 21.4 | 0.000 |
| 6726.667 | 26.00 | 4.607 | –1.03 | 0.482E-30 | 47.7 | 47.5 | 0.001 |
| 6750.152 | 26.00 | 2.4241 | –2.621 | 0.411E-31 | 74.2 | 74.0 | 0.001 |
| 6810.263 | 26.00 | 4.607 | –0.986 | 0.450E-30 | 51.0 | 50.3 | 0.000 |
| 6837.006 | 26.00 | 4.593 | –1.687 | 0.246E-31 | 18.1 | 18.2 | 0.001 |
| 4508.288 | 26.10 | 2.8557 | –2.44 | 0.956E-32 | 84.8 | 84.2 | |
| 4520.224 | 26.10 | 2.8068 | –2.65 | 0.857E-32 | 81.1 | 81.1 | |
| 4576.340 | 26.10 | 2.8443 | –2.95 | 0.943E-32 | 62.5 | 62.3 | |
| 4620.521 | 26.10 | 2.8283 | –3.21 | 0.930E-32 | 53.6 | 53.9 | |
| 5197.577 | 26.10 | 3.2306 | –2.22 | 0.869E-32 | 81.0 | 80.0 | |
| 5234.625 | 26.10 | 3.2215 | –2.18 | 0.869E-32 | 83.1 | 82.5 | |
| 5264.812 | 26.10 | 3.2304 | –3.13 | 0.943E-32 | 44.4 | 44.4 | |
| 5414.073 | 26.10 | 3.2215 | –3.58 | 0.930E-32 | 28.1 | 27.5 | |
| 5425.257 | 26.10 | 3.1996 | –3.22 | 0.845E-32 | 40.9 | 41.7 | |
| 6369.462 | 26.10 | 2.8912 | –4.11 | 0.742E-32 | 19.7 | 19.1 | |
| 6432.680 | 26.10 | 2.8912 | –3.57 | 0.742E-32 | 42.8 | 41.2 | |
| 7711.724 | 26.10 | 3.9034 | –2.50 | 0.930E-32 | 47.4 | 47.3 | |
| 5052.167 | 06.0 | 7.685 | –1.24 | 2.80 | 34.4 | 33.0 | –0.001 |
| 5380.337 | 06.0 | 7.685 | –1.57 | 2.80 | 22.3 | 21.7 | 0.000 |

**Table 3.** continued.

| Wavelength (Å) | ion | $\chi_{exc}$ (eV) | $\log gf$ | $C_6$ | EW HIP 56948 | EW Sun | ΔNLTE (dex) |
|---|---|---|---|---|---|---|---|
| 6587.61 | 06.0 | 8.537 | –1.05 | 2.80 | 14.1 | 13.9 | 0.000 |
| 7111.47 | 06.0 | 8.640 | –1.07 | 0.291E-29 | 11.0 | 11.2 | 0.000 |
| 7113.179 | 06.0 | 8.647 | –0.76 | 0.297E-29 | 22.5 | 22.1 | 0.000 |
| 7771.944 | 08.0 | 9.146 | 0.37 | 0.841E-31 | 70.7 | 68.7 | 0.000 |
| 7774.166 | 08.0 | 9.146 | 0.22 | 0.841E-31 | 61.2 | 59.8 | –0.001 |
| 7775.388 | 08.0 | 9.146 | 0.00 | 0.841E-31 | 49.1 | 48.8 | –0.002 |
| 4751.822 | 11.0 | 2.1044 | –2.078 | 2.80 | 13.5 | 13.7 | 0.000 |
| 5148.838 | 11.0 | 2.1023 | –2.044 | 2.80 | 10.9 | 10.9 | 0.001 |
| 6154.225 | 11.0 | 2.1023 | –1.547 | 2.80 | 39.1 | 38.3 | –0.002 |
| 6160.747 | 11.0 | 2.1044 | –1.246 | 2.80 | 55.5 | 54.0 | 0.002 |
| 5711.088 | 12.0 | 4.345 | –1.729 | 2.80 | 106.1 | 105.3 | –0.002 |
| 6318.717 | 12.0 | 5.108 | –1.945 | 2.80 | 38.6 | 38.3 | 0.000 |
| 6319.236 | 12.0 | 5.108 | –2.165 | 2.80 | 28.5 | 28.3 | 0.001 |
| 6696.018 | 13.0 | 3.143 | –1.481 | 2.80 | 40.6 | 40.4 | 0.000 |
| 6698.667 | 13.0 | 3.143 | –1.782 | 2.80 | 22.5 | 22.3 | –0.002 |
| 5488.983 | 14.0 | 5.614 | –1.69 | 2.80 | 20.6 | 20.4 | |
| 5645.611 | 14.0 | 4.929 | –2.04 | 2.80 | 37.0 | 35.6 | |
| 5684.484 | 14.0 | 4.953 | –1.55 | 2.80 | 63.6 | 62.1 | |
| 5690.425 | 14.0 | 4.929 | –1.77 | 2.80 | 49.8 | 48.9 | |
| 5701.104 | 14.0 | 4.930 | –1.95 | 2.80 | 40.1 | 38.9 | |
| 5793.073 | 14.0 | 4.929 | –1.96 | 2.80 | 44.7 | 44.4 | |
| 6125.021 | 14.0 | 5.614 | –1.50 | 2.80 | 33.3 | 32.0 | |
| 6145.015 | 14.0 | 5.616 | –1.41 | 2.80 | 41.0 | 39.1 | |
| 6243.823 | 14.0 | 5.616 | –1.27 | 2.80 | 47.5 | 46.8 | |
| 6244.476 | 14.0 | 5.616 | –1.32 | 2.80 | 48.6 | 47.4 | |
| 6721.848 | 14.0 | 5.862 | –1.12 | 2.80 | 46.1 | 45.4 | |
| 6741.63 | 14.0 | 5.984 | –1.65 | 2.80 | 16.9 | 16.8 | |
| 6046.000 | 16.0 | 7.868 | –0.15 | 2.80 | 19.4 | 19.5 | |
| 6052.656 | 16.0 | 7.870 | –0.4 | 2.80 | 12.7 | 12.7 | |
| 6743.54 | 16.0 | 7.866 | –0.6 | 2.80 | 9.4 | 9.1 | |
| 6757.153 | 16.0 | 7.870 | –0.15 | 2.80 | 18.8 | 18.3 | |
| 7698.974 | 19.0 | 0.000 | –0.168 | 0.104E-30 | 158.3 | 158.6 | 0.000 |
| 4512.268 | 20.0 | 2.526 | –1.901 | 2.80 | 23.3 | 22.5 | |
| 5260.387 | 20.0 | 2.521 | –1.719 | 0.727E-31 | 32.6 | 32.6 | |
| 5512.980 | 20.0 | 2.933 | –0.464 | 2.80 | 89.1 | 86.9 | 0.001 |
| 5590.114 | 20.0 | 2.521 | –0.571 | 0.636E-31 | 92.5 | 91.3 | –0.001 |
| 5867.562 | 20.0 | 2.933 | –1.57 | 2.80 | 24.3 | 24.2 | 0.000 |
| 6166.439 | 20.0 | 2.521 | –1.142 | 0.595E-30 | 70.4 | 70.1 | –0.001 |
| 6169.042 | 20.0 | 2.523 | –0.797 | 0.595E-30 | 93.3 | 92.4 | 0.000 |
| 6455.598 | 20.0 | 2.523 | –1.34 | 0.509E-31 | 57.4 | 56.5 | |
| 6471.662 | 20.0 | 2.525 | –0.686 | 0.509E-31 | 92.8 | 92.2 | 0.000 |
| 6499.650 | 20.0 | 2.523 | –0.818 | 0.505E-31 | 87.2 | 85.4 | –0.001 |
| 6798.470 | 20.0 | 2.709 | –2.45 | 2.80 | 7.7 | 7.3 | |
| 4743.821 | 21.0 | 1.4478 | 0.35 | 0.597E-31 | 9.7 | 9.8 | |
| 5081.57 | 21.0 | 1.4478 | 0.30 | 2.80 | 7.9 | 8.2 | |
| 5520.497 | 21.0 | 1.8649 | 0.55 | 2.80 | 6.8 | 6.8 | |
| 5671.821 | 21.0 | 1.4478 | 0.55 | 2.80 | 15.6 | 15.3 | |
| 4420.661 | 21.1 | 0.6184 | –2.273 | 2.80 | 16.2 | 16.5 | |
| 5657.87 | 21.1 | 1.507 | –0.30 | 2.80 | 69.4 | 67.3 | |
| 5684.19 | 21.1 | 1.507 | –0.95 | 2.80 | 39.5 | 38.2 | |
| 6245.63 | 21.1 | 1.507 | –1.030 | 2.80 | 34.2 | 33.8 | |
| 6279.76 | 21.1 | 1.500 | –1.2 | 2.80 | 30.8 | 29.8 | |
| 6300.698 | 21.1 | 1.507 | –2.0 | 2.80 | 5.9 | 5.6 | |
| 6320.843 | 21.1 | 1.500 | –1.85 | 2.80 | 9.9 | 9.3 | |
| 6604.578 | 21.1 | 1.3569 | –1.15 | 2.80 | 37.1 | 36.6 | |
| 4281.369 | 22.0 | 0.8129 | –1.359 | 0.502E-31 | 24.6 | 24.4 | –0.001 |
| 4465.802 | 22.0 | 1.7393 | –0.163 | 0.398E-31 | 38.1 | 37.9 | –0.001 |

**Table 3.** continued.

| Wavelength (Å) | ion | $\chi_{exc}$ (eV) | $\log gf$ | $C_6$ | EW HIP 56948 | EW Sun | ΔNLTE (dex) |
|---|---|---|---|---|---|---|---|
| 4758.120 | 22.0 | 2.2492 | 0.425 | 0.384E-31 | 42.6 | 42.9 | –0.001 |
| 4759.272 | 22.0 | 2.2555 | 0.514 | 0.386E-31 | 46.4 | 46.3 | 0.000 |
| 5022.871 | 22.0 | 0.8258 | –0.434 | 0.358E-31 | 70.1 | 69.8 | 0.002 |
| 5113.448 | 22.0 | 1.443 | –0.783 | 0.306E-31 | 27.3 | 27.6 | –0.002 |
| 5219.700 | 22.0 | 0.021 | –2.292 | 0.208E-31 | 29.3 | 29.0 | –0.002 |
| 5490.150 | 22.0 | 1.460 | –0.933 | 0.541E-31 | 21.6 | 21.4 | –0.003 |
| 5866.452 | 22.0 | 1.066 | –0.840 | 0.216E-31 | 47.5 | 47.9 | 0.002 |
| 6126.217 | 22.0 | 1.066 | –1.424 | 0.206E-31 | 22.1 | 22.2 | –0.001 |
| 6258.104 | 22.0 | 1.443 | –0.355 | 0.481E-31 | 51.9 | 51.4 | –0.003 |
| 6261.101 | 22.0 | 1.429 | –0.479 | 0.468E-31 | 49.5 | 48.7 | –0.003 |
| 4583.408 | 22.1 | 1.165 | –2.87 | 2.80 | 31.3 | 31.4 | 0.000 |
| 4636.33 | 22.1 | 1.16 | –3.152 | 2.80 | 19.2 | 19.1 | 0.000 |
| 4657.212 | 22.1 | 1.243 | –2.8 | 2.80 | 32.4 | 32.2 | 0.000 |
| 4865.611 | 22.1 | 1.116 | –2.81 | 2.80 | 40.3 | 39.3 | 0.000 |
| 4911.193 | 22.1 | 3.123 | –0.537 | 2.80 | 51.6 | 51.8 | –0.002 |
| 5211.54 | 22.1 | 2.59 | –1.49 | 2.80 | 34.2 | 33.0 | –0.001 |
| 5381.015 | 22.1 | 1.565 | –1.97 | 2.80 | 61.1 | 59.9 | 0.000 |
| 5418.767 | 22.1 | 1.582 | –2.11 | 2.80 | 49.5 | 48.8 | 0.001 |
| 4594.119 | 23.0 | 0.068 | –0.67 | 0.216E-31 | 55.6 | 55.8 | |
| 4875.486 | 23.0 | 0.040 | –0.81 | 0.198E-31 | 45.9 | 45.4 | |
| 5670.85 | 23.0 | 1.080 | –0.42 | 0.358E-31 | 19.5 | 19.2 | |
| 5727.046 | 23.0 | 1.081 | –0.011 | 0.435E-31 | 39.4 | 38.9 | |
| 6039.73 | 23.0 | 1.063 | –0.65 | 0.398E-31 | 13.8 | 13.1 | |
| 6081.44 | 23.0 | 1.051 | –0.578 | 0.389E-31 | 14.7 | 14.4 | |
| 6090.21 | 23.0 | 1.080 | –0.062 | 0.398E-31 | 33.8 | 33.1 | |
| 6119.528 | 23.0 | 1.064 | –0.320 | 0.389E-31 | 23.4 | 22.6 | |
| 6199.20 | 23.0 | 0.286 | –1.28 | 0.196E-31 | 14.6 | 14.6 | |
| 6251.82 | 23.0 | 0.286 | –1.34 | 0.196E-31 | 16.2 | 15.3 | |
| 6274.65 | 23.0 | 0.267 | –1.67 | 0.194E-31 | 9.2 | 8.5 | |
| 6285.160 | 23.0 | 0.275 | –1.51 | 0.194E-31 | 11.2 | 10.8 | |
| 4801.047 | 24.0 | 3.1216 | –0.130 | 0.452E-31 | 49.2 | 49.4 | –0.003 |
| 4936.335 | 24.0 | 3.1128 | –0.25 | 0.432E-31 | 44.3 | 44.3 | –0.003 |
| 5238.964 | 24.0 | 2.709 | –1.27 | 0.519E-31 | 16.5 | 16.3 | –0.002 |
| 5247.566 | 24.0 | 0.960 | –1.59 | 0.392E-31 | 81.3 | 81.1 | –0.003 |
| 5272.007 | 24.0 | 3.449 | –0.42 | 0.315E-30 | 24.6 | 24.0 | –0.003 |
| 5287.20 | 24.0 | 3.438 | –0.87 | 0.309E-30 | 11.4 | 11.5 | –0.003 |
| 5783.09 | 24.0 | 3.323 | –0.43 | 0.802E-30 | 31.8 | 31.2 | –0.002 |
| 4588.199 | 24.1 | 4.071 | –0.594 | 2.80 | 70.8 | 69.7 | –0.003 |
| 4592.049 | 24.1 | 4.073 | –1.252 | 2.80 | 47.5 | 47.7 | –0.002 |
| 5237.328 | 24.1 | 4.073 | –1.087 | 2.80 | 54.0 | 54.0 | 0.000 |
| 5246.767 | 24.1 | 3.714 | –2.436 | 2.80 | 16.1 | 15.5 | 0.001 |
| 5502.067 | 24.1 | 4.168 | –2.049 | 2.80 | 19.3 | 18.7 | 0.000 |
| 4082.939 | 25.0 | 2.1782 | –0.354 | 0.255E-31 | 90.0 | 89.8 | –0.007 |
| 4739.10 | 25.0 | 2.9408 | –0.490 | 0.352E-31 | 61.5 | 60.3 | –0.002 |
| 5004.891 | 25.0 | 2.9197 | –1.63 | 0.314E-31 | 14.0 | 14.1 | –0.004 |
| 6013.49 | 25.0 | 3.073 | –0.251 | 2.80 | 87.8 | 86.5 | –0.005 |
| 6016.64 | 25.0 | 3.073 | –0.084 | 2.80 | 97.0 | 96.1 | –0.006 |
| 6021.79 | 25.0 | 3.076 | +0.034 | 2.80 | 89.5 | 89.3 | –0.005 |
| 5212.691 | 27.0 | 3.5144 | –0.11 | 0.339E-30 | 21.4 | 20.6 | –0.002 |
| 5247.911 | 27.0 | 1.785 | –2.08 | 0.327E-31 | 18.1 | 17.7 | –0.001 |
| 5483.352 | 27.0 | 1.7104 | –1.49 | 0.289E-31 | 51.1 | 51.2 | –0.002 |
| 5530.774 | 27.0 | 1.710 | –2.23 | 0.226E-31 | 18.9 | 19.1 | –0.002 |
| 5647.23 | 27.0 | 2.280 | –1.56 | 0.414E-31 | 15.0 | 14.7 | –0.002 |
| 6189.00 | 27.0 | 1.710 | –2.46 | 0.206E-31 | 11.6 | 11.3 | –0.002 |
| 6454.995 | 27.0 | 3.6320 | –0.25 | 0.378E-30 | 14.7 | 14.1 | –0.002 |
| 5589.358 | 28.0 | 3.898 | –1.14 | 0.398E-30 | 27.6 | 27.0 | |
| 5643.078 | 28.0 | 4.164 | –1.25 | 0.379E-30 | 16.1 | 15.7 | |

**Table 3.** continued.

| Wavelength (Å) | ion | $\chi_{exc}$ (eV) | $\log gf$ | $C_6$ | EW HIP 56948 | EW Sun | ΔNLTE (dex) |
|---|---|---|---|---|---|---|---|
| 6086.282 | 28.0 | 4.266 | –0.51 | 0.406E-30 | 45.7 | 44.9 | |
| 6108.116 | 28.0 | 1.676 | –2.44 | 0.248E-31 | 64.3 | 63.3 | |
| 6130.135 | 28.0 | 4.266 | –0.96 | 0.391E-30 | 24.4 | 23.6 | |
| 6204.604 | 28.0 | 4.088 | –1.14 | 0.277E-30 | 23.1 | 22.4 | |
| 6223.984 | 28.0 | 4.105 | –0.98 | 0.393E-30 | 28.7 | 28.3 | |
| 6378.25 | 28.0 | 4.1535 | –0.90 | 0.391E-30 | 32.5 | 31.8 | |
| 6767.772 | 28.0 | 1.826 | –2.17 | 2.80 | 79.9 | 79.2 | |
| 6772.315 | 28.0 | 3.657 | –0.99 | 0.356E-30 | 50.6 | 50.0 | |
| 7727.624 | 28.0 | 3.678 | –0.4 | 0.343E-30 | 91.4 | 90.7 | |
| 7788.930 | 28.0 | 1.950 | –2.0 | 0.218E-31 | 92.7 | 92.1 | |
| 7797.586 | 28.0 | 3.89 | –0.34 | 2.80 | 80.0 | 78.6 | |
| 5105.541 | 29.0 | 1.39 | –1.516 | 2.80 | 91.5 | 91.5 | |
| 5218.197 | 29.0 | 3.816 | 0.476 | 2.80 | 52.2 | 51.2 | |
| 5220.066 | 29.0 | 3.816 | –0.448 | 2.80 | 17.3 | 17.3 | |
| 7933.13 | 29.0 | 3.79 | –0.368 | 2.80 | 30.5 | 30.8 | |
| 4722.159 | 30.0 | 4.03 | –0.38 | 2.80 | 71.9 | 71.2 | –0.001 |
| 4810.534 | 30.0 | 4.08 | –0.16 | 2.80 | 73.8 | 73.3 | –0.001 |
| 6362.35 | 30.0 | 5.79 | 0.14 | 2.80 | 21.6 | 21.1 | 0.000 |
| 4854.867 | 39.1 | 0.9923 | –0.38 | 2.80 | 48.3 | 48.4 | |
| 4883.685 | 39.1 | 1.0841 | 0.07 | 2.80 | 57.6 | 57.1 | |
| 4900.110 | 39.1 | 1.0326 | –0.09 | 2.80 | 55.5 | 55.3 | |
| 5087.420 | 39.1 | 1.0841 | –0.17 | 2.80 | 49.1 | 48.4 | |
| 5200.413 | 39.1 | 0.9923 | –0.57 | 2.80 | 39.0 | 38.6 | |
| 4050.320 | 40.1 | 0.713 | –1.06 | 2.80 | 23.8 | 23.4 | 0.001 |
| 4208.980 | 40.1 | 0.713 | –0.51 | 2.80 | 43.2 | 42.0 | 0.000 |
| 4442.992 | 40.1 | 1.486 | –0.42 | 2.80 | 25.7 | 24.7 | 0.000 |
| 5853.67 | 56.1 | 0.604 | –0.91 | 0.53E-31 | 64.6 | 63.7 | –0.002 |
| 6141.71 | 56.1 | 0.704 | –0.08 | 0.53E-31 | 116.2 | 115.7 | 0.000 |
| 6496.90 | 56.1 | 0.604 | –0.38 | 0.53E-31 | 99.5 | 99.2 | 0.000 |

**Table 4.** Stellar parameters and Li abundance of HIP 56948 relative to the Sun (HIP 56948 – Sun).

| $\Delta T_{\rm eff}$ (K) | $\Delta \log g$ (dex) | $\Delta$[Fe/H] (dex) | $\Delta v_t$ (km s$^{-1}$) | $\Delta$Li (NLTE) (dex) | $\Delta v \sin i$ (km s$^{-1}$) | Method | Reference |
|---|---|---|---|---|---|---|---|
| $17 \pm 7$ | $+0.02 \pm 0.02$ | $+0.02 \pm 0.01$ | $+0.01 \pm 0.01$ | $0.23 \pm 0.05$ | $+0.01 \pm 0.03$ | spectroscopy | This work |
| $26 \pm 70$ | $-0.07 \pm 0.07$ | | | | | IRFM, Hipparcos | L. Casagrande (priv. comm.) |
| $26 \pm 63$ | | | | | | IRFM | Casagrande et al. (2011) |
| $24 \pm 25^a$ | | | | | | IRFM | Casagrande et al. (2010) |
| $17 \pm 5$ | $+0.01 \pm 0.01$ | $+0.02 \pm 0.01$ | $-0.01 \pm 0.01$ | 0.22 | $+0.05$ | spectroscopy | Takeda & Tajitsu (2009) |
| $3 \pm 5$ | $-0.02 \pm 0.01$ | $+0.01 \pm 0.01$ | $-0.01 \pm 0.04$ | | | spectroscopy | Takeda & Tajitsu (2009) |
| $60 \pm 56$ | $+0.03 \pm 0.08$ | $+0.04 \pm 0.03$ | | $0.22 \pm 0.07$ | $0.0 \pm 0.1$ | spectroscopy | Ramírez et al. (2009) |
| $5 \pm 36$ | $-0.04 \pm 0.05$ | $+0.01 \pm 0.02$ | $+0.01 \pm 0.06$ | $-0.02 \pm 0.13$ | $0.0 \pm 0.1$ | spectroscopy | Meléndez & Ramírez (2007) |
| $-2 \pm 52$ | | | | | | photometry | Masana et al. (2006) |

**Notes.** $^{(a)}$ Error bar based only on photometric errors.

**Table 5.** Atomic and molecular line list in the vicinity of the Li lines.

| Wavelength Å | Species | $\chi_{exc}$ (eV) | log $gf$ (dex) |
|---|---|---|---|
| 6706.5476 | CN | 3.13 | −1.359 |
| 6706.5665 | CN | 2.19 | −1.650 |
| 6706.657 | CN | 0.860 | −2.993 |
| 6706.658 | CN | 0.614 | −3.622 |
| 6706.728 | CN | 0.625 | −2.400 |
| 6706.7329 | CN | 0.870 | −1.768 |
| 6706.8440 | CN | 1.96 | −2.775 |
| 6706.8626 | CN | 2.07 | −1.882 |
| 6706.880 | Fe II | 5.956 | −4.103 |
| 6707.00 | Si I | 5.954 | −2.56 |
| 6707.172 | Fe I | 5.538 | −2.810 |
| 6707.2052 | CN | 1.97 | −1.222 |
| 6707.272 | CN | 2.177 | −1.416 |
| 6707.2823 | CN | 2.055 | −1.349 |
| 6707.300 | $C_2$ | 0.933 | −1.717 |
| 6707.3706 | CN | 3.05 | −0.522 |
| 6707.433 | Fe I | 4.608 | −2.25 |
| 6707.460 | CN | 0.788 | −3.094 |
| 6707.461 | CN | 0.542 | −3.730 |
| 6707.4695 | CN | 1.88 | −1.581 |
| 6707.473 | Sm II | 0.933 | −1.91 |
| 6707.548 | CN | 0.946 | −1.588 |
| 6707.5947 | CN | 1.89 | −1.451 |
| 6707.596 | Cr I | 4.208 | −2.667 |
| 6707.6453 | CN | 0.946 | −3.330 |
| 6707.660 | $C_2$ | 0.926 | −1.743 |
| 6707.7561 | $^7$Li | 0.000 | −0.428 |
| 6707.7682 | $^7$Li | 0.000 | −0.206 |
| 6707.809 | CN | 1.221 | −1.935 |
| 6707.8475 | CN | 3.60 | −2.417 |
| 6707.8992 | CN | 3.36 | −3.110 |
| 6707.9066 | $^7$Li | 0.000 | −1.509 |
| 6707.9080 | $^7$Li | 0.000 | −0.807 |
| 6707.9187 | $^7$Li | 0.000 | −0.807 |
| 6707.9196 | $^6$Li | 0.000 | −0.479 |
| 6707.9200 | $^7$Li | 0.000 | −0.807 |
| 6707.9230 | $^6$Li | 0.000 | −0.178 |
| 6707.9300 | CN | 1.98 | −1.651 |
| 6707.970 | $C_2$ | 0.920 | −1.771 |
| 6707.980 | CN | 2.372 | −3.527 |
| 6708.023 | Si I | 6.00 | −2.80 |
| 6708.0261 | CN | 1.98 | −2.031 |
| 6708.0728 | $^6$Li | 0.000 | −0.303 |
| 6708.094 | V I | 1.218 | −2.922 |
| 6708.099 | Ce II | 0.701 | −2.120 |
| 6708.1470 | CN | 1.87 | −1.884 |
| 6708.282 | Fe I | 4.988 | −2.70 |
| 6708.3146 | CN | 2.64 | −1.719 |
| 6708.347 | Fe I | 5.486 | −2.58 |
| 6708.3700 | CN | 2.64 | −2.540 |
| 6708.420 | CN | 0.768 | −3.358 |
| 6708.534 | Fe I | 5.558 | −2.936 |
| 6708.5407 | CN | 2.50 | −1.876 |
| 6708.577 | Fe I | 5.446 | −2.684 |

**Table 6.** Stellar abundances [X/H] in LTE and NLTE, and errors due to uncertainties in the stellar parameters.

| Element | LTE | NLTE | $\Delta T_{\rm eff}$ +7K | $\Delta\log g$ +0.02 dex | $\Delta v_t$ +0.01 km s$^{-1}$ | $\Delta$[Fe/H] +0.01 dex | param[a] | obs[b] | total[c] |
|---|---|---|---|---|---|---|---|---|---|
| | (dex) | (dex) | (dex) | (dex) | (dex) | (dex) | (dex) | (dex) | (dex) |
| C | 0.007 | 0.007 | –0.004 | 0.003 | 0.000 | 0.000 | 0.005 | 0.006 | 0.008 |
| O | 0.012 | 0.011 | –0.005 | 0.001 | –0.001 | 0.002 | 0.006 | 0.008 | 0.010 |
| Na | 0.014 | 0.014 | 0.004 | 0.000 | 0.000 | –0.001 | 0.004 | 0.006 | 0.007 |
| Mg | 0.013 | 0.012 | 0.004 | –0.002 | –0.001 | –0.001 | 0.005 | 0.005 | 0.007 |
| Al | 0.011 | 0.010 | 0.004 | 0.000 | 0.000 | –0.001 | 0.004 | 0.008 | 0.009 |
| Si | 0.022 | | 0.002 | 0.001 | –0.001 | 0.001 | 0.003 | 0.003 | 0.004 |
| S | 0.004 | | –0.003 | 0.003 | 0.000 | 0.001 | 0.004 | 0.005 | 0.007 |
| K | 0.007 | 0.007 | 0.006 | –0.007 | –0.002 | 0.001 | 0.009 | 0.009 | 0.013 |
| Ca | 0.024 | 0.023 | 0.005 | –0.002 | –0.002 | 0.000 | 0.006 | 0.003 | 0.006 |
| Sc | 0.025 | | 0.000 | 0.007 | –0.001 | 0.003 | 0.008 | 0.004 | 0.009 |
| Ti | 0.018 | 0.017 | 0.007 | 0.001 | –0.002 | –0.001 | 0.007 | 0.002 | 0.008 |
| V | 0.033 | | 0.008 | 0.002 | –0.001 | –0.001 | 0.008 | 0.004 | 0.009 |
| Cr | 0.015 | 0.012 | 0.005 | 0.000 | –0.002 | –0.001 | 0.005 | 0.003 | 0.006 |
| Mn | 0.021 | 0.016 | 0.006 | –0.003 | –0.003 | 0.000 | 0.007 | 0.005 | 0.009 |
| Fe | 0.020 | 0.021 | 0.006 | 0.000 | –0.002 | 0.000 | 0.006 | 0.001 | 0.006 |
| Co | 0.026 | 0.024 | 0.005 | 0.002 | –0.001 | 0.000 | 0.005 | 0.003 | 0.006 |
| Ni | 0.025 | | 0.004 | 0.000 | –0.002 | 0.000 | 0.004 | 0.001 | 0.005 |
| Cu | 0.014 | | 0.005 | 0.000 | –0.002 | 0.000 | 0.005 | 0.005 | 0.007 |
| Zn | 0.019 | 0.018 | 0.001 | 0.001 | –0.003 | 0.002 | 0.004 | 0.005 | 0.006 |
| Y | 0.021 | | 0.001 | 0.007 | –0.004 | 0.003 | 0.009 | 0.004 | 0.010 |
| Zr | 0.041 | 0.041 | 0.002 | 0.008 | –0.002 | 0.003 | 0.009 | 0.005 | 0.010 |
| Ba | 0.024 | 0.023 | 0.002 | 0.002 | –0.004 | 0.005 | 0.007 | 0.005 | 0.009 |

**Notes.** [a] Adding errors in stellar parameters. [b] Observational errors. [c] Total error (stellar parameters and observational).

# Appendix A: Is the $T_{cond}$-abundance trend real?

We are just starting the era of high precision (0.01 dex) abundances studies, therefore the casual reader may question how real or universal is the abundance trend (⟨solar twins⟩ – Sun) with condensation temperature. The trend was first found by Meléndez et al. (2009), who determined a Spearman correlation coefficient of $r_S$ = +0.91 and a negligible probability of only ∼$10^{-9}$ of this trend to happen by pure chance. These results, based on Southern solar twins observed at the Magellan telescope, are reproduced in the left-upper panel of Fig. A.1, where the average abundance ratios of the solar twins is plotted against condensation temperature. Additional independent works are also shown in Fig. A.1, where a line representing the mean trend found by Meléndez et al. (2009), is superimposed upon the different samples.

The independent study by Ramírez et al. (2009), using McDonald data of Northern solar twins, follows the same trend (Fig. A.1, upper-right panel), as well as the average of six independent samples (Reddy et al. 2003; Allende Prieto et al. 2004; Takeda 2007; Neves et al. 2009; Gonzalez et al. 2010, Bensby et al., in prep.) of solar analogs in the literature (Ramírez et al. 2010), as shown in the left-middle panel of Fig. A.1.

The revision and extension (González Hernández et al. 2010) of the abundance analysis by Neves et al. (2009) of the HARPS high precision planet survey, also follows the same trend, except for a minor global shift of only −0.004 dex, as illustrated in the right-middle panel of Fig. A.1. In this panel we show the average abundance ratios[17] of 15 HARPS solar twins with $T_{eff}$, log $g$ and [Fe/H] within ±100 K, ±0.1 dex and ±0.1 dex of the Sun's stellar parameters. The agreement between the solar twin pattern of González Hernández et al. (2010) and the mean trend of Meléndez et al. (2009) is good, except for the element O and to a lesser extent for S, for which it is difficult to determine precise abundances. In particular, notice that González Hernández et al. (2010) derived oxygen abundances from the [OI] 630 nm line, which is badly blended with NiI. Also, notice that the [OI] feature is the weakest employed by them. Since their oxygen abundance is based on a single line, which is the weakest of all features analyzed by them, and that [OI] is blended with NiI, it is natural to expect that the O abundances in González Hernández et al. (2010) have the largest uncertainties. Furthermore, the HARPS spectra taken for planet hunting show some contamination from the calibration arc, so that abundances derived from only one single feature should be taken with care.

Regarding the analysis of individual stars, most of them also display the abundance trend, as shown for example for four solar twins in Fig. 2 of Ramírez et al. (2009) and 11 solar twins in Fig. 4 of Meléndez et al. (2009). Two new examples are shown in Fig. A.1. In the bottom-left panel we show the average abundance of the pair of solar analogs 16 Cyg A and B (Ramírez et al. 2011), based on high resolution ($R = 60\,000$) and high S/N (∼400) McDonald observations. As can be seen, this pair also follows the abundance trend, after a minor shift of −0.015 dex. In the bottom-right panel we show the abundance ratios of the solar twin 18 Sco (Meléndez et al. 2012, in prep.), based on high quality ($R = 110\,000$, $S/N ∼ 800$) UVES/VLT data. It is clear that the abundance trend is also followed by 18 Sco, after a shift of only +0.014 dex in the abundance ratios. Similar results are obtained using HIRES/Keck data (Meléndez et al. 2012, in prep.; see also Appendix B).
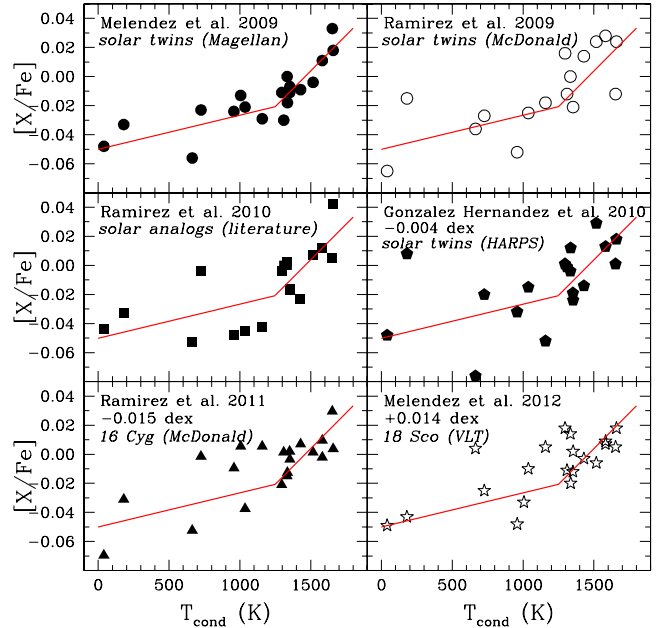
---

[17] The individual abundance ratios with errors larger than 0.1 dex were discarded from the data of González Hernández et al. (2010) when computing the average [X/Fe] values.

**Fig. A.1.** [X/Fe] ratios (from carbon to zinc) vs. condensation temperature for different samples of solar twins and solar analogs. The solid line represents the mean trend found by Meléndez et al. (2009). *upper-left* (filled circles): Southern sample of solar twins by Meléndez et al. (2009); *upper-right* (open circles): Northern solar twin sample by Ramírez et al. (2009); *middle-left* (squares): average of six different literature samples of solar analogs (Ramírez et al. 2010); *middle-right* (pentagons): average of 15 solar twins in the HARPS sample of González Hernández et al. (2010), after a shift of −0.004 dex; *lower-left* (triangles): average of the pair of solar analogs 16 Cyg A and B (Ramírez et al. 2011), after a shift of −0.015 dex; *lower-right* (stars): abundance pattern of the solar twin 18 Sco (Meléndez et al. 2012, in prep.), after a shift of +0.014 dex.

Thus, all recent high precision abundance studies based on different samples of solar twins and solar analogs in the Southern and Northern skies, using different instrumentation (Tull Coude Spectrograph at McDonald, MIKE at Magellan, HARPS at La Silla, UVES at the VLT, HIRES at Keck), show the abundance trend. In conclusion, it seems that the reality of the abundance trend found by Meléndez et al. (2009) and Ramírez et al. (2009), is well established.

# Appendix B: Test of our precision using the asteroids Juno and Ceres

The referee suggested that we test our method using observations of two asteroids of different properties, obtained with the same instrument and setup, in order to show whether our very small standard errors (∼0.005 dex) are adequate to estimate the observational uncertainties, as well as to look for potential systematic problems with the asteroid Ceres. Although we have not acquired such data yet, we do have observations of the solar twin 18 Sco and two different asteroids observed with different instruments: high quality UVES spectra of 18 Sco and the asteroid Juno ($R = 110\,000$ and $S/N ∼ 800$) and high quality HIRES spectra of 18 Sco and the asteroid Ceres ($R = 100\,000$, $S/N ∼ 400$). Juno is a S-type asteroid and Ceres is a C-type asteroid (e.g., DeMeo et al. 2009), therefore they have very different spectral properties and the relative analysis of 18 Sco to both Juno and Ceres should reveal if there is any problem in using their reflected solar light.
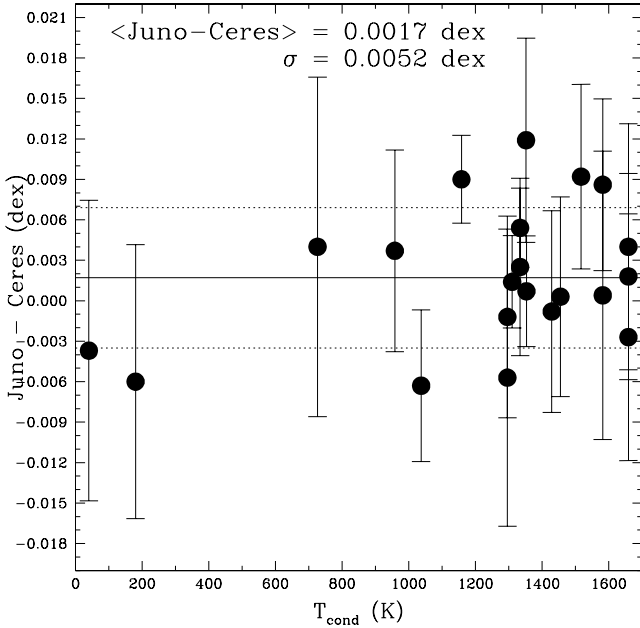
**Fig. B.1.** Differences between the solar abundances obtained with the asteroids Juno and Ceres, obtained from (Juno – Ceres) = [X/H] (18 Sco – Ceres) – [X/H](18 Sco – Juno). The solid line shows the mean difference and the dotted lines show the element-to-element scatter.
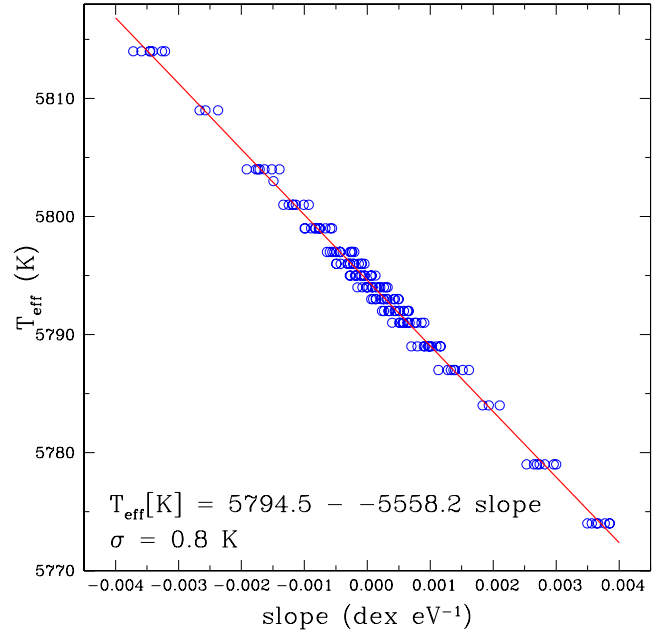


**Fig. C.1.** $T_{\rm eff}$ as a function of the slope = $d(\delta A_i^{\rm FeI})/d(\chi_{\rm exc})$ (see Eq. (2)), for a range of surface gravities (4.40 dex $\leq \log g \leq$ 4.52 dex), corresponding to a scatter of only 0.8 K in $T_{\rm eff}$. The results of different model atmospheres are shown as open circles. The line represents a linear fit.

The analysis has been performed as described in Sect. 3. Our preliminary LTE results for the stellar parameters of 18 Sco are $T_{\rm eff}$ = 5831 ± 10 K, $\log g$ = 4.46 ± 0.02 dex, [Fe/H] = 0.06 ± 0.01 dex. Full details of the abundance analysis will be published elsewhere. In Fig. B.1 we show the difference between the [X/H] ratios obtained in 18 Sco using the Ceres and Juno asteroids, $[X/H]_{\rm 18Sco-Ceres} - [X/H]_{\rm 18Sco-Juno}$, or in other words the abundance difference (Juno – Ceres). Notice that the same set of lines was used for both analyses. The error bars shown in Fig. B.1 are the combined error bar based on the standard error (s.e.) of each analysis, i.e., error = $\sqrt{s.e._{\rm 18Sco-Ceres}^2 + s.e._{\rm 18Sco-Juno}^2}$.

As can be seen, the standard errors fully explain the small deviations of the (Juno–Ceres) abundance ratios. The mean difference ⟨Juno – Ceres⟩ is only 0.0017 dex, and the element-to-element scatter is only 0.0052 dex, meaning that each of the individual analyses should have typical errors of about 0.003–0.004 dex. The agreement is very satisfactory considering the different instrumentation employed and that the comparison between Juno and Ceres is done through a third object (the solar twin 18 Sco). Also, notice that there is no meaningful trend with condensation temperature. The test performed here strongly supports for our high precision and removes the possibility that the abundance trend may arise due to the particular properties of asteroids.

Besides the potential applications of high precision differential abundance techniques to study the star-planet connection, these techniques are also giving new insights in other areas. Nissen & Schuster (2010) achieved uncertainties of 0.03 dex in [Mg/Fe] and only 0.02 dex in both [Ca/Fe] and [Ti/Fe], showing a clear separation of the halo into two distinct populations with different [α/Fe] ratios. Regarding globular clusters, Meléndez & Cohen (2009) have shown that CN-weak giants in M71 show a star-to-star scatter in [O/Fe] and [Ni/Fe] of only 0.018 dex, while [Mg/Fe] and [La/Fe] have a scatter of 0.015 dex. The star-to-star scatter in metallicity ([Fe/H]) is only 0.025 dex. Even a

lower star-to-star scatter is found among "globular cluster star twins" (stars within ±100 K of a globular cluster standard star) of NGC 6752. Using superb spectra ($R$ = 110 000; $S/N$ = 500) obtained with UVES on the VLT (Yong et al. 2003, 2005) and applying similar techniques to those presented in Sect. 3, Yong et al. (in prep.) have found an unprecedentedly low star-to-star scatter of only 0.003 dex in the iron abundances among NGC 6752 star twins, revealing chemical homogeneity in this cluster at the 0.7% level.

## Appendix C: Determination of stellar parameters

As mentioned in Sect. 3, the excitation and ionization equilibrium do not depend only on $T_{\rm eff}$ and $\log g$, respectively. There is some dependence with other stellar parameters, but to a much lesser extent, such that a "unique" solution can easily be obtained after a few iterations. In practice, considering the weak degeneracies, a first guess of the effective temperature can be obtained by computing the slope at three different $T_{\rm eff}$ (e.g., in steps of 50 K and at fixed solar $\log g$) at the best microturbulence velocity (at a given $T_{\rm eff}$ and $\log g$). Then a linear fit is performed to $T_{\rm eff}$ vs. slope (see Fig. C.1) to find the effective temperature at slope = 0. Then, for this $T_{\rm eff}$ we can run three models with different $\log g$ (e.g., in steps of 0.05 dex in $\log g$) in order to find the best surface gravity, by fitting $\log g$ vs. $\Delta^{\rm II-I}$ (see Fig. C.2), and for each model the microturbulence is obtained. This leads to the first guess of $T_{\rm eff}$, $\log g$ and $v_t$. Further iterations at smaller steps (down to 1 K in $T_{\rm eff}$, 0.01 dex in $\log g$ and 0.01 km s$^{-1}$ in $v_t$) can quickly lead to the best solution that simultaneously satisfies the conditions of differential spectroscopic equilibrium (Eqs. (2)–(4)).

In Fig. C.1 we show that the excitation equilibrium provides a precise $T_{\rm eff}$. In this figure, effective temperature is plotted versus the slope = $d(\delta A_i^{\rm FeI})/d(\chi_{\rm exc})$. As can be seen, there is a clear linear relation between $T_{\rm eff}$ and the slope, with some minor spread of only 0.8 K due to a range in adopted surface gravities.
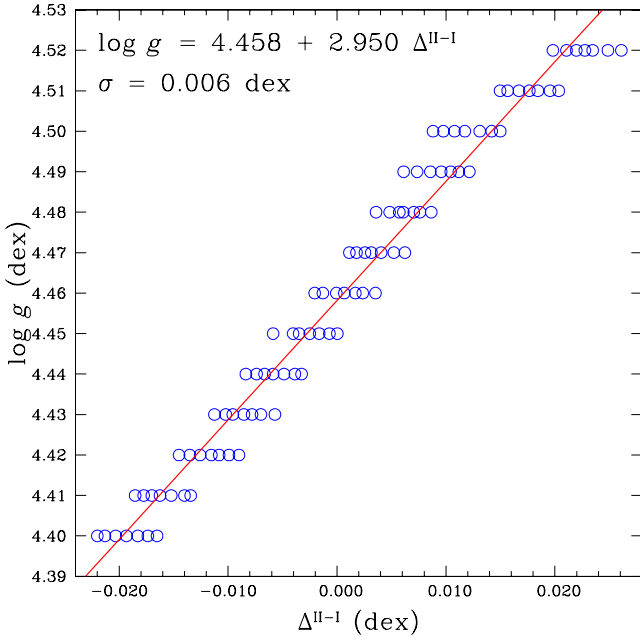
**Fig. C.2.** Surface gravity vs. $\Delta^{\mathrm{II-I}} = (3\Delta^{\mathrm{FeII-FeI}} + 2\Delta^{\mathrm{TiII-TiI}} + \Delta^{\mathrm{CrII-CrI}})/6$ (see Eq. (3)). The spread of the circles corresponds to a range of effective temperatures (5791 K $\leq T_{\mathrm{eff}} \leq$ 5797 K), implying a scatter of 0.006 dex in $\log g$. The line represents a linear fit.

Regarding the ionization equilibrium, we show in Fig. C.2 the dependence between surface gravity and $\Delta^{\mathrm{II-I}}$ (see Eq. (3)). A linear fit represents this relation well, with a scatter in $\log g$ of only 0.006 dex for models in a range of effective temperatures.

In Fig. C.3 we show the linear dependence between microturbulence velocity and the slope $\mathrm{d}(\delta A_i^{\mathrm{FeI}})/\mathrm{d}(EW_r)$. For a given model, $v_t$ could be constrained to within 0.0004 km s$^{-1}$. A range in $T_{\mathrm{eff}}$ (5791 K $\leq T_{\mathrm{eff}} \leq$ 5797 K) and $\log g$ (4.40 dex $\leq \log g \leq$ 4.52 dex) imply in a scatter of only 0.009 km s$^{-1}$ in $v_t$.

Given the above dependences, the stellar parameters $T_{\mathrm{eff}}$, $\log g$ and $v_t$ must be iteratively modified until the spectroscopic equilibrium conditions (Eqs. (2)–(4)) are satisfied simultaneously. Since the degeneracy is relatively small, the final solution ($T_{\mathrm{eff}}/\log g/v_t$ = 5794 K/4.46 dex/1.00 km s$^{-1}$) is very close to the independent solutions shown in Figs. C.1–C.3 (5794.5 K/4.458 dex/1.006 km s$^{-1}$).

In order to check how unique the derived final solution is, we have run over 200 models with different stellar parameters, with a very fine grid (steps of only 1 K in $T_{\mathrm{eff}}$ and 0.01 dex in $\log g$) near our best solution. We then evaluated how close to zero are the slope in $T_{\mathrm{eff}}$ (Eq. (2)) and the ionization equilibrium parameter $\Delta^{\mathrm{II-II}}$ (Eq. (3)). The following quantity is evaluated for each model,

$$TG = (|slope/error| + |\Delta^{\mathrm{II-II}}/error|)/2. \qquad (\mathrm{C.1})$$

The model showing the lowest $TG$ value would be the best spectroscopic solution, which in our case is obtained for $T_{\mathrm{eff}}$ = 5794 K, $\log g$ = 4.46 dex, and $v_t$ = 1.00 km s$^{-1}$. A contour plot for the $TG$ parameter is shown in Fig. C.4. Besides the best solution at $T_{\mathrm{eff}}$ = 5794 K and $\log g$ = 4.46 dex, there are a few other nearby plausible solutions, with a mean value at $T_{\mathrm{eff}}$ = 5794.3 ± 0.5 K and $\log g$ = 4.462 ± 0.012 dex, shown by a cross in Fig. C.4. Our grid samples a much larger coverage than that shown in Fig. C.4, and we have verified that the best solution indeed represents a global minimum, i.e., there is no other solution that can simultaneously satisfy the conditions of differential
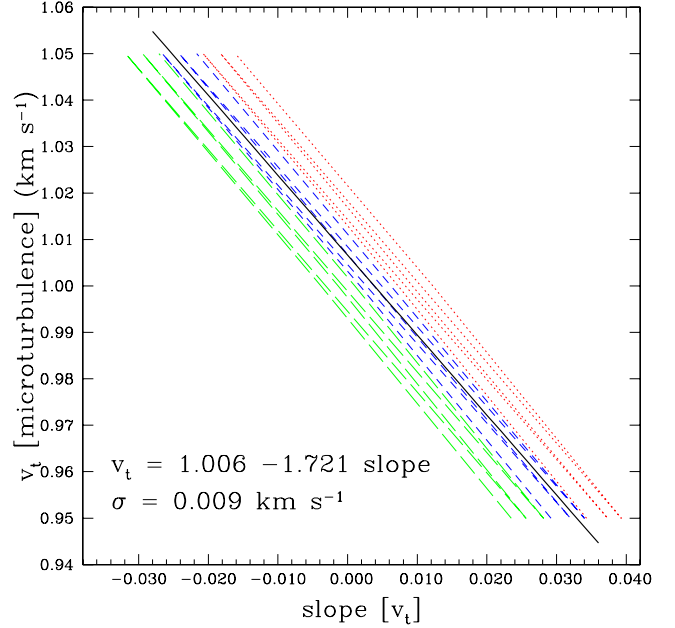
**Fig. C.3.** Microturbulence velocity vs. slope $\mathrm{d}(\delta A_i^{\mathrm{FeI}})/\mathrm{d}(EW_r)$ (see Eq. (4)). The dotted, dashed and long dashed lines are for $T_{\mathrm{eff}}$ = 5791, 5794, 5797 K, respectively, and the spread shown for each line style is due to a range in $\log g$ (4.40 dex $\leq \log g \leq$ 4.52 dex). This spread in $T_{\mathrm{eff}}$ and $\log g$ corresponds to a scatter of 0.009 km s$^{-1}$ in $v_t$. The solid line represents a linear fit.
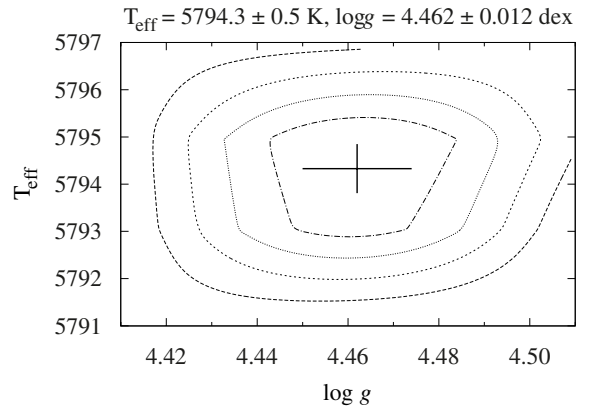


**Fig. C.4.** Contour plot of the parameter $TG$ (Eq. (C.1)), which evaluates how good the differential spectroscopic equilibrium is. The minimum is shown by a cross at $T_{\mathrm{eff}}$ = 5794.3 ± 0.5 K and $\log g$ = 4.462 ± 0.012 dex, which is in excellent agreement with our adopted solution. The contour levels increase in steps of $\Delta TG$ = 0.1 from the minimum.

spectroscopic equilibrium. Thus, within the error bars our solution is "unique".

## Appendix D: Helium abundance and the age and $\log g$ of HIP 56948

Since our stellar parameters are very precise, the He abundance in HIP 56948 actually cannot be arbitrarily different from the solar He abundance. For example, an evolutionary track computed with a He abundance 5% higher than solar, would shift the $T_{\mathrm{eff}}$ by about +74 K at the same $\log g$, i.e., a change 10 times larger than our error bar in $T_{\mathrm{eff}}$, thus leading to no plausible solutions. We are currently building an extensive grid of models with He as a free parameter, using the Dartmouth stellar evolution code
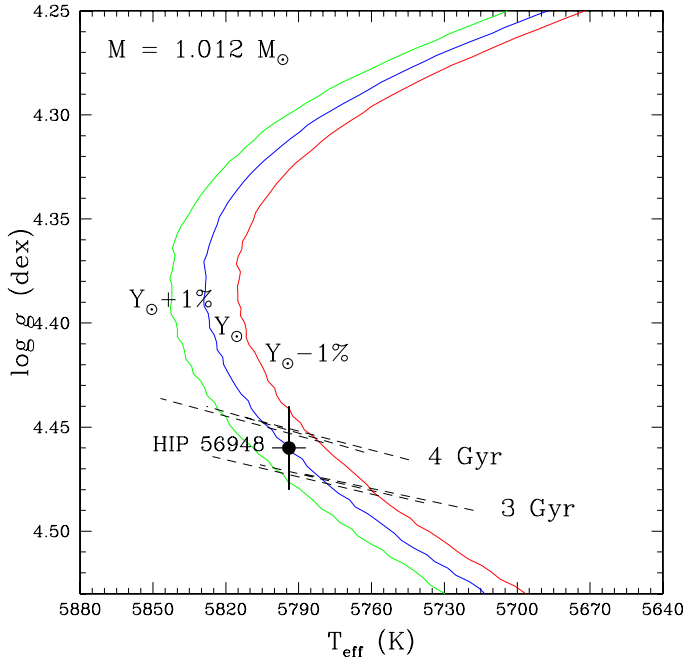
**Fig. D.1.** Solar metallicity evolutionary tracks for 1.012 $M_\odot$ (solid lines) at three different He abundances: solar and ±1% solar. Isochrones at 3 and 4 Gyr are plotted with dashed lines. The position of HIP 56948 and error bars in $T_{eff}$ and $\log g$ are also shown.

(Chaboyer et al. 2001; Guenther et al. 1992), which is based upon the Yale stellar evolution code.

In Fig. D.1, we show evolutionary tracks for $M = 1.012\,M_\odot$ (solid lines), which is the best mass found for HIP 56948 using the Dartmouth tracks, adopting the He solar abundance. These models were computed at three different helium abundances, solar and ±1% solar. We also show isochrones at 3 and 4 Gyr for different He abundances. The error bars in $\log g$ and $T_{eff}$ put constraints on the He abundance, which can not be radically different from solar. Notice that the isochrones run parallel to each other and with only a minor shift for a change of ±1% in the He abundance, thus resulting in about the same central solution for age, independent of the adopted He content. Therefore thanks to our small error bars in stellar parameters we can put stringent constraints on the age of HIP 56948. Interestingly, there is a degeneracy between He and mass, although below our 2% error bar in mass.

Another example where the adoption of a somewhat different He abundance did not affect the stellar age much is for the pair of solar analogs 16 Cyg A and B. For this pair, asteroseismology have recently constrained the ages of these stars, which are in excellent agreement with those derived from our isochrone technique, despite the somewhat different adopted He abundances. Based on three months of almost uninterrupted Kepler observations, Metcalfe et al. (2012) obtained an age = 6.8 ± 0.4 Gyr for their optimal models, in excellent agreement with an age = 7.1 ± 0.4 Gyr derived from our isochrone technique for the 16 Cyg pair (Ramírez et al. 2011).

The effect of changing He by ±1% (in Y) in our model atmospheres has also a minor impact on the derived spectroscopic $\log g$. As shown by Stromgren et al. (1982), for solar type dwarfs

the change in $\log g$ due to a change in the helium to hydrogen ratio ($y = N_{He}/N_{H}$) is:

$$\log g = \log g' + \log \left[\frac{(1 + 4y')(1 + y)}{(1 + 4y)(1 + y')}\right]. \tag{D.1}$$

Lind et al. (2011b) have shown that the relation above is also adequate for giant stars. For a change of +1% in Y in HIP 56948, the predicted change in $\log g$ is only −0.001 dex, which is well below our error bar in $\log g$ (0.02 dex). Thus, assuming that the He abundance of HIP 56948 is not radically different from solar, our derived spectroscopic $\log g$ value is essentially unaffected.

## Appendix E: $v \sin i$ and macroturbulence velocity

We have determined $v \sin i$ from the differential line broadening (HIP 56948 – Sun). Naively we could be assuming an identical macroturbulence for both stars, but at a given luminosity class, macroturbulence seems a smooth function of temperature (e.g., Saar & Osten 1997; Gray 2005; Valenti & Fischer 2005), so neglecting this effect can lead to a slight overestimation of $v \sin i$ in HIP 56948 because it is hotter than the Sun and therefore the contribution of $v_{macro}$ to the line broadening in HIP 56948 should be slightly larger.

The trend of macroturbulence velocity with $T_{eff}$ described by Gray (2005) for main sequence stars[18] can be fitted by

$$v_{macro} = 13.499 - 0.00707\,T_{eff} + 9.2422 \times 10^{-7} T_{eff}^2. \tag{E.1}$$

A similar correlation was advocated by Valenti & Fischer (2005) (after normalization to $v_{macro}^\odot = 3.50$ km s$^{-1}$, which is the value obtained for the Sun using Gray's relation):

$$v_{macro} = 3.50 + (T_{eff} - 5777)/650. \tag{E.2}$$

Finally, the mean relation (active and non-active stars) obtained by Saar & Osten (1997), after transforming $(B - V)$ to $T_{eff}$ (Valenti & Fischer 2005) and normalizing it to $v_{macro}^\odot = 3.50$ km s$^{-1}$, is:

$$v_{macro} = 3.50 + (T_{eff} - 5777)/388. \tag{E.3}$$

The first two relations are valid for ∼5000–6500 K, while the last relation is valid for ∼5000–6100 K. On average, the above relations predict a differential (HIP 56948 – Sun) $\Delta v_{macro} = 0.044 \pm 0.018$ km s$^{-1}$.

In order to determine $v \sin i$ we selected 19 lines in the 602−682 nm region, although essentially similar results are obtained (albeit with ever so slightly larger errors) when 50 lines covering the 446–682 nm region are used. First, we performed spectral synthesis of selected lines, in order to calibrate the relation between line width (in Å) and total broadening (in km s$^{-1}$). Then, we estimated the total broadening using a much larger set of lines, and obtained $v \sin i$ after subtracting both the instrumental and the macroturbulence broadening.

After taking into account the somewhat higher macroturbulence velocity of HIP 56948, we find $v \sin i/v \sin i_\odot = 1.006 \pm 0.014$, or $\Delta v \sin i = +0.013 \pm 0.026$ km s$^{-1}$ (or ±0.032 km s$^{-1}$ including the error in macroturbulence), i.e., HIP 56948 seems to have about the same rotation velocity as the Sun, or rotating slightly faster, although it is unclear how much faster due to the uncertain $\sin i$ factor.

---

[18] For subgiants, giants and luminous giants, our fits can be found in Hekker & Meléndez (2007).